

International Journal of Modern Physics A
 © World Scientific Publishing Company

Modified trimaximal mixing for solar and reactor neutrino mixing angles

Yulin Chen

*Graduate School of Science, Tokai University,
 4-1-1 Kitakaname, Hiratsuka, Kanagawa 259-1292, Japan*

Yuta Hyodo

*Graduate School of Science and Technology, Tokai University,
 4-1-1 Kitakaname, Hiratsuka, Kanagawa 259-1292, Japan*

Micro/Nano Technology Center, Tokai University, 4-1-1 Kitakaname, Hiratsuka, Kanagawa 259-1292, Japan

Teruyuki Kitabayashi*

*Department of Physics, Tokai University,
 4-1-1 Kitakaname, Hiratsuka, Kanagawa 259-1292, Japan
 teruyuki@tokai-u.jp*

Received Day Month Year
 Revised Day Month Year

The trimaximal mixing scheme is one of the widely studied neutrino mixing schemes. However, the predicted solar neutrino mixing angle θ_{12} and the reactor neutrino mixing angle θ_{13} cannot simultaneously realize their best-fit values. To address this issue, a minimal modification to the trimaximal mixing scheme is proposed. The modified trimaximal mixing scheme can simultaneously predict the best-fit values of θ_{12} and θ_{13} using an additional real parameter introduced via the modification.

PACS numbers:14.60.Pq

1. Introduction

Numerous neutrino mixing matrices and textures related to flavor mass matrix have been proposed previously, including tri-bi maximal mixing (TBM),^{1–4} texture zeros,^{5–45} $\mu - \tau$ symmetric texture,^{46–77} magic texture,^{78–86} and textures and mixings under discrete symmetries, e.g., A_n and S_n .⁸⁷

The trimaximal mixing scheme is a widely studied neutrino mixing scheme.^{88–91, 91–94, 94–103} There are versions of the trimaximal texture. In this paper, we focus on the so-called TM1 and TM2 mixings. The predicted values of neutrino

*Corresponding author

mixing angles using TM1 and TM2 are consistent with the observations. However, the predicted solar neutrino mixing angle θ_{12} and reactor neutrino mixing angle θ_{13} cannot simultaneously realize their best-fit values. In the case of TM2, the predicted value of θ_{12} approaches the upper limit of the 3σ allowed region. Hence, the TM2 mixing scheme may soon be excluded from neutrino oscillation experiments.

Although simultaneous reproducibility of θ_{12} and θ_{13} cannot be realized using the TM1 and TM2 mixing schemes, these schemes still garner research attention. The most interesting feature of TM1 and TM2 is related to the Z_2 symmetry. The flavor neutrino mass matrices in the TM1 and TM2 mixing schemes are invariant under the exact Z_2 symmetry.⁸² Thus, modifying the TM1 and TM2 mixing schemes to realize the simultaneous reproducibility of θ_{12} and θ_{13} using the exact Z_2 symmetry is an important research topic neutrino physics. Although, we have attempted to construct new modified TM1 and TM2 mixing schemes using the exact Z_2 symmetry, we have not yet succeeded. However, constructing a modified version of TM1 and TM2 mixing schemes that do not adhere to the Z_2 symmetry is also important.

In this study, modified TM1 and TM2 mixing schemes are constructed using the following strategy:

- Improving the simultaneous reproducibility of θ_{12} and θ_{13} is the highest priority.
- Z_2 symmetry breaking is allowed.
- We modify the original TM1 mixing matrix U_1 and TM2 mixing matrix U_2 by introducing a matrix A_i , resulting in the modified mixing matrix $\tilde{U}_i = A_i U_i$ ($i = 1, 2$). Usually, the modified mixing matrix \tilde{U}_i is nonunitary.^{104–108} However, because the original TM1 and TM2 mixing schemes are constructed based on unitary arguments,⁹⁴ the unitarity of the modified TM1 and TM2 mixing matrices needs to be maintained.
- Minimize the number of parameters in the matrix A_i to realize the minimal modification of TM1 and TM2.

We successfully derived the modified TM1 and TM2 mixing matrices. These modified matrices simultaneously predict the best-fit values of θ_{12} and θ_{13} using the additional real parameter.

The remaining sections of this study are structured as follows. Section 2 provides an overview of model-independent useful formulas and observed data related to neutrinos. Additionally, this section highlights the key features of the TM1 and TM2 mixing schemes. Section 3 outlines the methodology employed for modifying the TM1 and TM2 mixings. The successful modification of TM1 and TM2 is presented in Sections 4 and 5, respectively. Lastly, Section 6 presents a summary of the obtained results and their implications.

2. Trimaximal mixing

2.1. Model-independent formulas and observations

The neutrino mixings are parametrized based on the Pontecorvo-Maki-Nakagawa-Sakata (PMNS) mixing matrix^{109–112}

$$U = \begin{pmatrix} U_{e1} & U_{e2} & U_{e3} \\ U_{\mu 1} & U_{\mu 2} & U_{\mu 3} \\ U_{\tau 1} & U_{\tau 2} & U_{\tau 3} \end{pmatrix}, \quad (1)$$

where

$$\begin{aligned} U_{e1} &= c_{12}c_{13}, & U_{e2} &= s_{12}c_{13}, & U_{e3} &= s_{13}e^{-i\delta}, \\ U_{\mu 1} &= -s_{12}c_{23} - c_{12}s_{23}s_{13}e^{i\delta}, \\ U_{\mu 2} &= c_{12}c_{23} - s_{12}s_{23}s_{13}e^{i\delta}, & U_{\mu 3} &= s_{23}c_{13}, \\ U_{\tau 1} &= s_{12}s_{23} - c_{12}c_{23}s_{13}e^{i\delta}, \\ U_{\tau 2} &= -c_{12}s_{23} - s_{12}c_{23}s_{13}e^{i\delta}, & U_{\tau 3} &= c_{23}c_{13}. \end{aligned} \quad (2)$$

In the abbreviations $s_{ij} = \sin \theta_{ij}$ and $c_{ij} = \cos \theta_{ij}$, $\theta_{ij} = \{\theta_{12}, \theta_{23}, \theta_{13}\}$ denote neutrino mixing angles. δ denotes the Dirac CP phase.

The sines and cosines of the three mixing angles can be obtained as follows:

$$s_{12}^2 = \frac{|U_{e2}|^2}{1 - |U_{e3}|^2}, \quad s_{23}^2 = \frac{|U_{\mu 3}|^2}{1 - |U_{e3}|^2}, \quad s_{13}^2 = |U_{e3}|^2. \quad (3)$$

The Jarlskog invariant J_{CP} ¹¹³ is derived based on the Dirac CP phase δ and the elements of the PMNS matrix. In standard parametrization, the Jarlskog invariant can be expressed as follows:

$$J_{\text{CP}} = \text{Im}(U_{e1}U_{e2}^*U_{\mu 1}^*U_{\mu 2}) = s_{12}s_{23}s_{13}c_{12}c_{23}s_{13}^2 \sin \delta. \quad (4)$$

A global analysis of the current data obtained from neutrino oscillation experiments yields the following best-fit values of the squared mass differences $\Delta m_{ij}^2 = m_i^2 - m_j^2$ related to the neutrino mass eigenstates $\{m_1, m_2, m_3\}$ and the mixing angles for the normal mass ordering (NO), $m_1 < m_2 < m_3$, as¹¹⁴

$$\begin{aligned} \frac{\Delta m_{21}^2}{10^{-5} \text{ eV}^2} &= 7.41^{+0.21}_{-0.20} \quad (6.82 \rightarrow 8.03), \\ \frac{\Delta m_{31}^2}{10^{-3} \text{ eV}^2} &= 2.507^{+0.026}_{-0.027} \quad (2.427 \rightarrow 2.590), \\ s_{12}^2 &= 0.303^{+0.012}_{-0.012} \quad (0.270 \rightarrow 0.341), \\ s_{23}^2 &= 0.451^{+0.019}_{-0.016} \quad (0.408 \rightarrow 0.603), \\ s_{13}^2 &= 0.02225^{+0.00056}_{-0.00059} \quad (0.02052 \rightarrow 0.02398), \\ \delta/\circ &= 232^{+36}_{-26} \quad (144 \rightarrow 350), \end{aligned} \quad (5)$$

where the \pm represents the 1σ region and the parentheses denote the 3σ region. For inverted mass ordering (IO), $m_3 < m_1 \simeq m_2$,

$$\begin{aligned} \frac{\Delta m_{21}^2}{10^{-5} \text{ eV}^2} &= 7.41^{+0.21}_{-0.20} \quad (6.82 \rightarrow 8.03), \\ \frac{\Delta m_{32}^2}{10^{-3} \text{ eV}^2} &= -2.486^{+0.025}_{-0.028} \quad (-2.570 \rightarrow -2.406), \\ s_{12}^2 &= 0.303^{+0.012}_{-0.011} \quad (0.270 \rightarrow 0.341), \\ s_{23}^2 &= 0.569^{+0.016}_{-0.021} \quad (0.412 \rightarrow 0.613), \\ s_{13}^2 &= 0.02223^{+0.00058}_{-0.00058} \quad (0.02048 \rightarrow 0.02416), \\ \delta/\circ &= 276^{+22}_{-29} \quad (194 \rightarrow 344). \end{aligned} \quad (6)$$

Herein, the observed values of θ_{12} are the same in the NO and IO cases. Furthermore, the observed values of θ_{13} are also nearly identical in the NO and IO cases. Therefore, we compare the model predictions of θ_{12} and θ_{13} based on these observed values in the NO case.

2.2. Trimaximal mixing

In this subsection, we provide a brief review of trimaximal mixing. The trimaximal mixing scheme is one of the modifications of the TBM. Since the predicted reactor mixing angle is not consistent with the observation in the TBM scheme, some modification of the TBM is required. It is a simple way to modify the TBM that the first or second column of the mixing matrix in the TBM is unchanged and the other two columns are modified. Such modification of the mixing matrix of the TBM can be realized by multiplying it from the right-hand side by a complex (2,3) or (1,3) rotation matrix. These types of modifications lead the so-called the first or second trimaximal mixing (TM1 or TM2).

Moreover, there is third trimaximal mixing (TM3). In the texture of TM3, the third column of the mixing matrix in the TBM is unchanged and the other two columns are modified (multiplying TBM mixing matrix from the right-hand side by a complex (1,2) rotation matrix). It is known that predicted reactor mixing angle to be zero for TM3. Therefore, the TM3 mixing is exclusion from neutrino oscillation experiments.

The mixing matrix of TM1 is given as follows:^a

$$U_1 = \begin{pmatrix} \sqrt{\frac{2}{3}} & \frac{\cos \theta}{\sqrt{3}} & \frac{\sin \theta}{\sqrt{3}} \\ -\frac{1}{\sqrt{6}} \frac{\cos \theta}{\sqrt{3}} - \frac{e^{i\phi} \sin \theta}{\sqrt{2}} & \frac{\sin \theta}{\sqrt{3}} + \frac{e^{i\phi} \cos \theta}{\sqrt{2}} \\ -\frac{1}{\sqrt{6}} \frac{\cos \theta}{\sqrt{3}} + \frac{e^{i\phi} \sin \theta}{\sqrt{2}} & \frac{\sin \theta}{\sqrt{3}} - \frac{e^{i\phi} \cos \theta}{\sqrt{2}} \end{pmatrix}, \quad (7)$$

^aAlthough the matrix U_1 does not have a “tri” column or row, we refer to U_1 as TM1 according to literature such as Ref.¹⁰³

yields the following mixing angles and the Dirac CP phase

$$s_{12}^2 = 1 - \frac{2}{3 - \sin^2 \theta}, \quad (8)$$

$$s_{23}^2 = \frac{1}{2} \left(1 + \frac{\sqrt{6} \sin 2\theta \cos \phi}{3 - \sin^2 \theta} \right), \quad (9)$$

$$s_{13}^2 = \frac{1}{3} \sin^2 \theta, \quad (10)$$

$$\tan \delta = \frac{5 + \cos 2\theta}{1 + 5 \cos 2\theta} \tan \phi. \quad (11)$$

In the term of θ_{13} , we obtain

$$s_{12}^2 = \frac{1 - 3s_{13}^2}{3(1 - s_{13}^2)}, \quad (12)$$

$$s_{23}^2 = \frac{1}{2} \left(1 + \frac{6\sqrt{2(1 - 3s_{13}^2)}s_{13} \cos \phi}{3(1 - s_{13}^2)} \right), \quad (13)$$

$$\tan \delta = \frac{1 - s_{13}^2}{1 - 5s_{13}^2} \tan \phi. \quad (14)$$

For TM2 mixing, the mixing matrix

$$U_2 = \begin{pmatrix} \sqrt{\frac{2}{3}} \cos \theta & \frac{1}{\sqrt{3}} & \sqrt{\frac{2}{3}} \sin \theta \\ -\frac{\cos \theta}{\sqrt{6}} + \frac{e^{-i\phi} \sin \theta}{\sqrt{2}} & \frac{1}{\sqrt{3}} & -\frac{\sin \theta}{\sqrt{6}} - \frac{e^{-i\phi} \cos \theta}{\sqrt{2}} \\ -\frac{\cos \theta}{\sqrt{6}} - \frac{e^{-i\phi} \sin \theta}{\sqrt{2}} & \frac{1}{\sqrt{3}} & -\frac{\sin \theta}{\sqrt{6}} + \frac{e^{-i\phi} \cos \theta}{\sqrt{2}} \end{pmatrix}, \quad (15)$$

yields the following mixing angles and the Dirac CP phase

$$s_{12}^2 = \frac{1}{3 - 2 \sin^2 \theta}, \quad (16)$$

$$s_{23}^2 = \frac{1}{2} \left(1 + \frac{\sqrt{3} \sin 2\theta \cos \phi}{3 - 2 \sin^2 \theta} \right), \quad (17)$$

$$s_{13}^2 = \frac{2}{3} \sin^2 \theta, \quad (18)$$

$$\tan \delta = \frac{2 + \cos 2\theta}{1 + 2 \cos 2\theta} \tan \phi, \quad (19)$$

as well as

$$s_{12}^2 = \frac{1}{3(1 - s_{13}^2)}, \quad (20)$$

$$s_{23}^2 = \frac{1}{2} \left(1 + \frac{3\sqrt{2 - 3s_{13}^2}s_{13} \cos \phi}{3(1 - s_{13}^2)} \right), \quad (21)$$

$$\tan \delta = \frac{1 - s_{13}^2}{1 - 2s_{13}^2} \tan \phi. \quad (22)$$

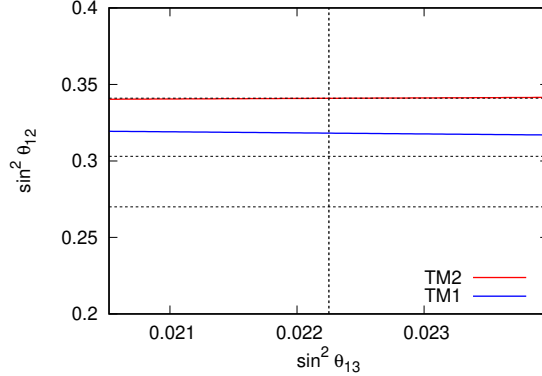


Fig. 1. The predicted values of θ_{12} and θ_{13} using TM1 and TM2 mixing schemes are depicted using blue and red colors, respectively. The upper, middle, and lower horizontal dotted lines represent the 3σ upper limit, the best-fit value, and the 3σ lower limit of θ_{12} in NO case, respectively. The vertical dotted line represents the best-fit value of θ_{13} in the NO case.

Figure 1 illustrates the predicted values of θ_{12} and θ_{13} using the TM1 (blue) and TM2 (red) mixing schemes. The upper, middle, and lower horizontal dotted lines represent the 3σ upper limit, best-fit value, and 3σ lower limit of θ_{12} in the NO case, respectively. The vertical dotted line denotes the best-fit value of θ_{13} in the NO case. Neither TM1 nor TM2 can simultaneously reproduce the best-fit values of θ_{12} and θ_{13} . In the case of TM2, the predicted value of θ_{12} approaches the upper limit of the 3σ allowed region.

Figure 2 depicts the predicted values of θ_{13} and θ_{23} using the TM1 and TM2 mixing schemes with respect to $\cos \phi = -0.3$ (upper panel) and $\cos \phi = 0.45$ (lower panel). The upper, middle, and lower horizontal dotted lines in each panel represent the 3σ upper limit, best-fit value, and 3σ lower limit of θ_{23} in the NO case for the upper panel and in the IO case for the lower panel. The vertical dotted line in both panels corresponds to the same value as depicted in Fig. 1. Figure 2 suggests that TM1 and TM2 can simultaneously reproduce the best-fit values of θ_{23} and θ_{13} by choosing an appropriate value of $\cos \phi$.

Moreover, the predicted value of the Dirac CP phase δ using TM1 and TM2 is based on ϕ . From Eq. (14) and Eq. (22), we obtain the following expression.

$$\tan \delta \sim \begin{cases} -6.9 \tan \phi & (\text{TM1}) \\ 1.4 \tan \phi & (\text{TM2}) \end{cases}. \quad (23)$$

2.3. Z_2 symmetry

The flavor neutrino mass matrix with TM2 mixing U_1 ,

$$M_1 = U_1^* D U_1^\dagger, \quad (24)$$

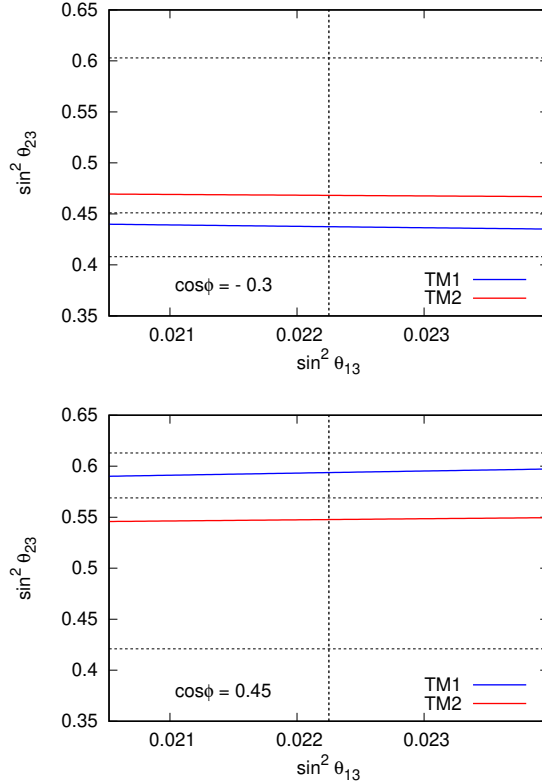


Fig. 2. Predicted values of θ_{13} and θ_{23} using the TM1 (blue) and TM2 (red) mixing schemes with respect to $\cos\phi = -0.3$ (upper panel) and $\cos\phi = 0.45$ (lower panel) are depicted. The upper, middle, and lower horizontal dotted lines in each panel represent the 3σ upper limit, best-fit value, and 3σ lower limit of θ_{23} in the NO case for the upper panel and in the IO case for the lower panel. The vertical dotted line in both panels corresponds to the same value as depicted in Fig. 1.

where $D = \text{diag.}(m_1, m_2, m_3)$, satisfies the Z_2 symmetry

$$S_1 M_1 S_1^T = M_1, \quad (25)$$

where

$$S_1 = \frac{1}{3} \begin{pmatrix} -1 & 2 & 2 \\ 2 & 2 & -1 \\ 2 & -1 & 2 \end{pmatrix}, \quad (26)$$

and $S_1^2 = S_1 S_1^T = S_1^T S_1 = 1$.

Similarly, the flavor neutrino mass matrix in the TM2 mixing scheme

$$M_2 = U_2^* D U_2^\dagger, \quad (27)$$

satisfies the Z_2 symmetry

$$S_2 M_2 S_2^T = M_2, \quad (28)$$

where

$$S_2 = \frac{1}{3} \begin{pmatrix} 1 & -2 & -2 \\ -2 & 1 & -2 \\ -2 & -2 & 1 \end{pmatrix}, \quad (29)$$

and $S_2^2 = S_2 S_2^T = S_2^T S_2 = 1$.

3. Modification methods

We modify the mixing matrix $U = \{U_1, U_2\}$ by introducing a matrix A as follows:

$$\tilde{U} = AU, \quad (30)$$

where

$$A = \begin{pmatrix} \alpha_{11} & \epsilon_{12} & \epsilon_{13} \\ \epsilon_{21} & \alpha_{22} & \epsilon_{23} \\ \epsilon_{31} & \epsilon_{32} & \alpha_{33} \end{pmatrix}, \quad (31)$$

with the conditions $|\alpha_{ii}| \leq 1$ and $|\alpha_{ii}| \gg |\epsilon_{ij}|$. In the case of $\alpha_{ij} = 1$ and $\epsilon_{ij} = 0$, we obtain the identity $A = \text{diag.}(1, 1, 1)$ and $\tilde{U} = U$.

In order to satisfy the unitarity condition for the modified mixing matrix \tilde{U} , it is necessary for the matrix A to be unitary:

$$AA^\dagger = A^\dagger A = 1. \quad (32)$$

To achieve modification with the minimum number of parameters, we assume that the matrix A is real. In addition, we consider scenarios where some of the elements ϵ_{ij} are set to zero. Having a greater number of zero elements in the matrix is advantageous as it reduces the number of parameters required. However, it should be noted that the case with all six zero elements is not allowed, as it would result in all ϵ_{ij} being zero, limiting the ability to modify the matrix.

Is it possible to have five zeros in the matrix A ? For example, if $\epsilon_{13} = \epsilon_{21} = \epsilon_{23} = \epsilon_{31} = \epsilon_{32} = 0$ and only ϵ_{12} is non-zero, then the matrix A is

$$A_{12} = \begin{pmatrix} \alpha_{11} & \epsilon_{12} & 0 \\ 0 & \alpha_{22} & 0 \\ 0 & 0 & \alpha_{33} \end{pmatrix}, \quad (33)$$

where the subscript of A indicates the position of the non-zero ϵ_{ij} . For A_{12} to be unitary, $\epsilon_{12} = 0$ is required. This is inconsistent with the five-zero condition. Thus, A_{12} should be excluded. Similarly, all five-zero matrices are excluded because they cannot simultaneously satisfy the unitarity and the five-zero conditions.

Among the possible configurations, there are six matrices that satisfy both the unitarity condition and the four-zero condition:

$$\begin{aligned} A_{12,21}^{(1)} &= \begin{pmatrix} \alpha & \epsilon & 0 \\ -\epsilon & \alpha & 0 \\ 0 & 0 & 1 \end{pmatrix} = \begin{pmatrix} \alpha & \sqrt{1-\alpha^2} & 0 \\ -\sqrt{1-\alpha^2} & \alpha & 0 \\ 0 & 0 & 1 \end{pmatrix}, \\ A_{12,21}^{(2)} &= \begin{pmatrix} \alpha & -\epsilon & 0 \\ \epsilon & \alpha & 0 \\ 0 & 0 & 1 \end{pmatrix} = \begin{pmatrix} \alpha & -\sqrt{1-\alpha^2} & 0 \\ \sqrt{1-\alpha^2} & \alpha & 0 \\ 0 & 0 & 1 \end{pmatrix}, \end{aligned} \quad (34)$$

$$\begin{aligned} A_{23,32}^{(1)} &= \begin{pmatrix} 1 & 0 & 0 \\ 0 & \alpha & \epsilon \\ 0 & -\epsilon & \alpha \end{pmatrix} = \begin{pmatrix} 1 & 0 & 0 \\ 0 & \alpha & \sqrt{1-\alpha^2} \\ 0 & -\sqrt{1-\alpha^2} & \alpha \end{pmatrix}, \\ A_{23,32}^{(2)} &= \begin{pmatrix} 1 & 0 & 0 \\ 0 & \alpha & -\epsilon \\ 0 & \epsilon & \alpha \end{pmatrix} = \begin{pmatrix} 1 & 0 & 0 \\ 0 & \alpha & -\sqrt{1-\alpha^2} \\ 0 & \sqrt{1-\alpha^2} & \alpha \end{pmatrix}, \end{aligned} \quad (35)$$

and

$$\begin{aligned} A_{13,31}^{(1)} &= \begin{pmatrix} \alpha & 0 & \epsilon \\ 0 & 1 & 0 \\ -\epsilon & 0 & \alpha \end{pmatrix} = \begin{pmatrix} \alpha & 0 & \sqrt{1-\alpha^2} \\ 0 & 1 & 0 \\ -\sqrt{1-\alpha^2} & 0 & \alpha \end{pmatrix}, \\ A_{13,31}^{(2)} &= \begin{pmatrix} \alpha & 0 & -\epsilon \\ 0 & 1 & 0 \\ \epsilon & 0 & \alpha \end{pmatrix} = \begin{pmatrix} \alpha & 0 & -\sqrt{1-\alpha^2} \\ 0 & 1 & 0 \\ \sqrt{1-\alpha^2} & 0 & \alpha \end{pmatrix}, \end{aligned} \quad (36)$$

where α denotes a real parameter ($0 \ll \alpha \leq 1$) and

$$\epsilon = \sqrt{1-\alpha^2}. \quad (37)$$

In the case of $\alpha = 1$, we obtain $\tilde{U} = U$.

Recall that the rotation matrix for 1-2 plane could be written as follows:

$$\begin{pmatrix} \cos \beta & -\sin \beta & 0 \\ \sin \beta & \cos \beta & 0 \\ 0 & 0 & 1 \end{pmatrix}. \quad (38)$$

By comparing Eq. (38) and Eq. (34), we can interpret $A_{12,21}^{(1)}$ and $A_{12,21}^{(2)}$ as matrices representing rotations in the 1-2 plane. Similarly, $A_{23,32}^{(1)}$ and $A_{23,32}^{(2)}$ ($A_{13,31}^{(1)}$ and $A_{13,31}^{(2)}$) can be considered as rotation matrices for the 2-3 (1-3) plane.

In conclusion, if we impose the condition of unitarity on the modified mixing matrix \tilde{U} , we can achieve a minimal modification of the original mixing matrix U

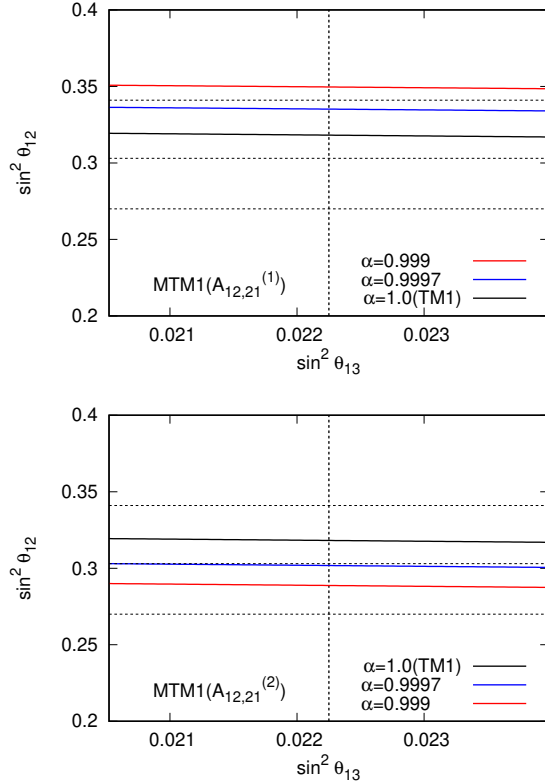


Fig. 3. Prediction of θ_{13} and θ_{12} in $\text{MTM1}(A_{12,21}^{(1)})$ and $\text{MTM1}(A_{12,21}^{(2)})$. The horizontal and vertical dotted lines in each panel are the same as in Fig. 1

by setting $\tilde{U} = AU$, where A is a matrix representing a certain rotation and has only one real parameter.^b

4. Modified TM1 mixing

4.1. $A_{12,21}^{(1)}$ and $A_{12,21}^{(2)}$

We modify TM1 mixing scheme using the rotation matrices $A_{12,21}^{(1)}$ and $A_{12,21}^{(2)}$ as follows:

$$\tilde{U}_1(A_{12,21}^{(1)}) = A_{12,21}^{(1)} U_1, \quad \tilde{U}_1(A_{12,21}^{(2)}) = A_{12,21}^{(2)} U_1. \quad (39)$$

^bWe use the parameter α to estimate the magnitude of the mixing matrix modification. However, the small parameter ϵ in Eq.(37) or β in Eq.(38) is also a good index to represent the magnitude of the modification.

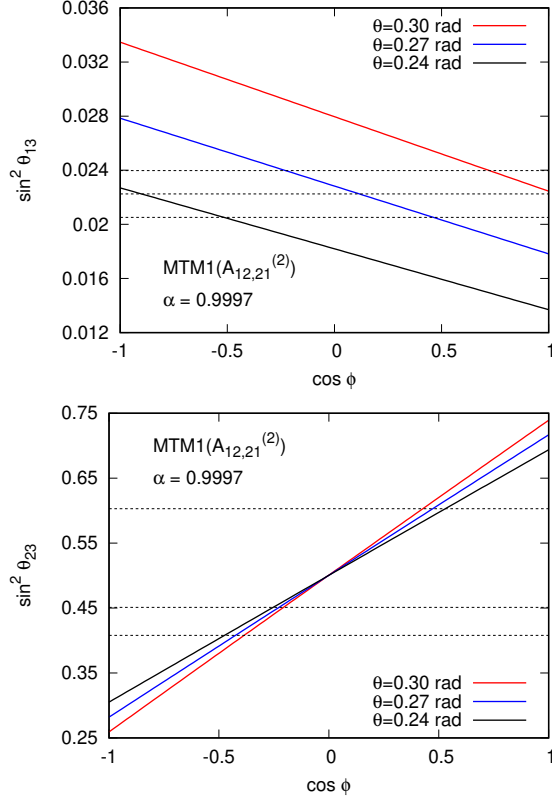


Fig. 4. The predicted values of θ_{13} (upper panel) and θ_{23} (lower panel) as a function of ϕ in the MTM1 ($A_{12,21}^{(2)}$). The upper, middle, and lower horizontal dotted lines represent the 3σ upper limit, the best-fit value, and the 3σ lower limit of θ_{13} (θ_{23}) in the NO (IO) case in the upper (lower) panel.

We term $\tilde{U}_1(A_{12,21}^{(1)})$ and $\tilde{U}_1(A_{12,21}^{(2)})$ as MTM1($A_{12,21}^{(1)}$) mixing and MTM1($A_{12,21}^{(2)}$) mixing, respectively. The mixing angles are

$$s_{12}^2 = \frac{5 \pm 4\alpha\sqrt{1-\alpha^2} - 3\alpha^2 - 6s_{13}^2}{6(1-s_{13}^2)}, \quad (40)$$

$$\begin{aligned} s_{23}^2 &= \frac{1}{6(1-s_{13}^2)} \left\{ 3\alpha^2 + (2 - 3\alpha^2 \mp 4\alpha\sqrt{1-\alpha^2}) \sin^2 \theta \right. \\ &\quad \left. + \sqrt{6}\alpha(\alpha \mp \sqrt{1-\alpha^2}) \sin 2\theta \cos \phi \right\}, \end{aligned}$$

$$s_{13}^2 = \frac{1}{6}(3 - 3\alpha^2 - B_1 + B_2), \quad (41)$$

where

$$\begin{aligned} B_1 &= (1 - 3\alpha^2 \mp 4\alpha\sqrt{1-\alpha^2}) \sin^2 \theta, \\ B_2 &= \sqrt{6}(1 - \alpha^2 \pm \alpha\sqrt{1-\alpha^2}) \sin 2\theta \cos \phi. \end{aligned} \quad (42)$$

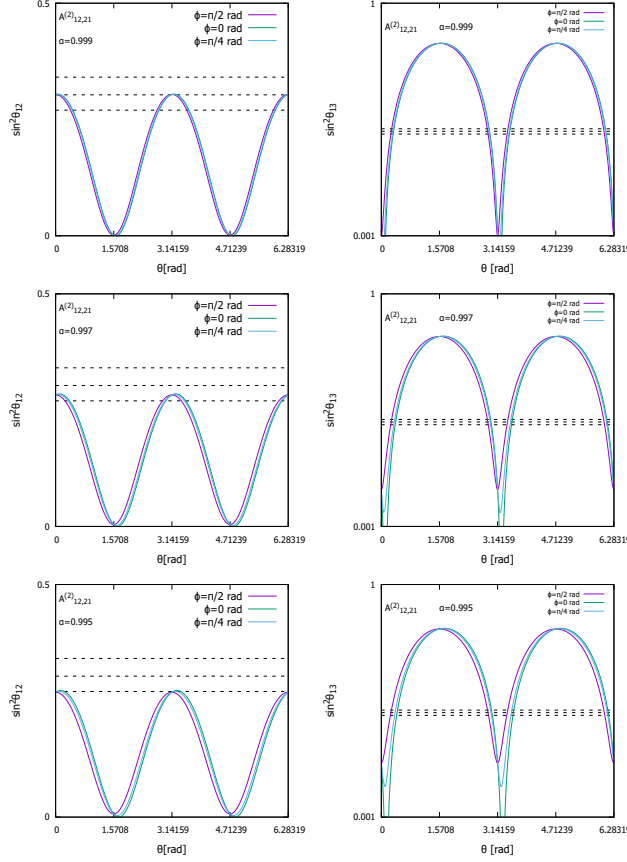
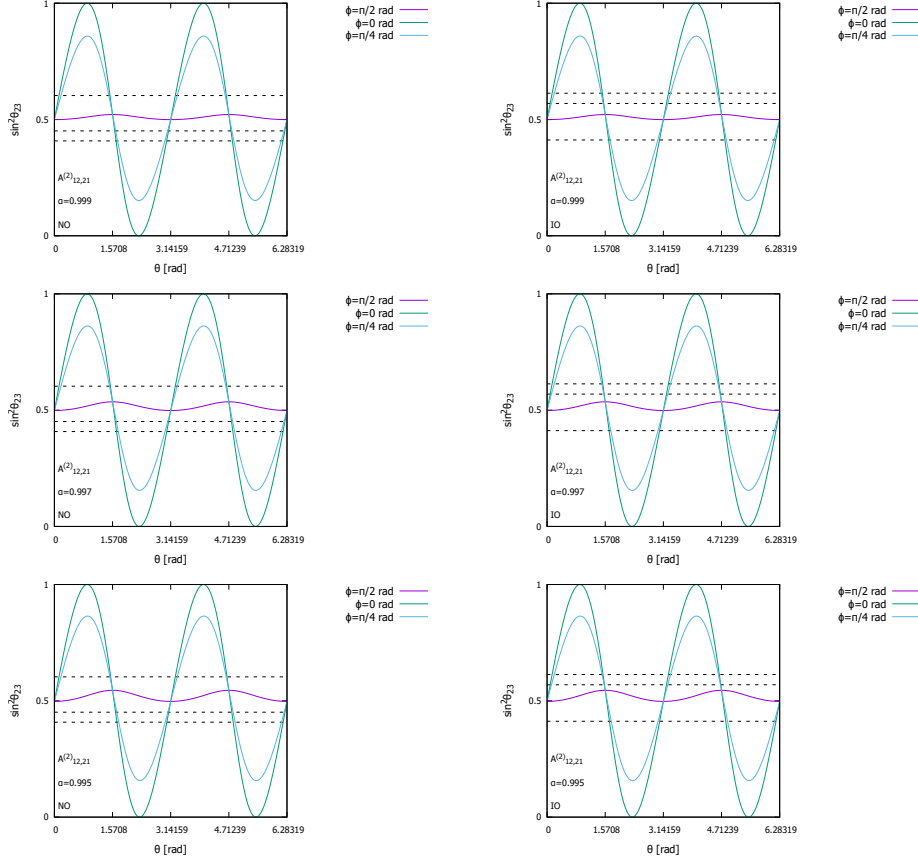


Fig. 5. s_{12}^2 (left-side panels) or s_{13}^2 (right-side panels) vs θ for ϕ [rad] = 0, $\frac{\pi}{4}$, $\frac{\pi}{2}$ in the case of MTM1($A_{12,21}^{(2)}$).

The upper sign of \pm and \mp must be considered in the case of MTM1($A_{12,21}^{(1)}$), and the lower sign of \pm and \mp must be considered in the case of MTM1($A_{12,21}^{(2)}$).

Figure 3 illustrates the predicted values of θ_{13} and θ_{12} based on the MTM1($A_{12,21}^{(1)}$) and MTM1($A_{12,21}^{(2)}$). The horizontal and vertical dotted lines in each panel represent the same parameters as those represented in Fig. 1. The upper panel indicates that the simultaneous reproducibility of θ_{12} and θ_{13} is diminished using the MTM1($A_{12,21}^{(1)}$). By contrast, the lower panel demonstrates that the simultaneous reproducibility of θ_{12} and θ_{13} is substantially enhanced using the MTM1($A_{12,21}^{(2)}$). For example, the best-fit values of θ_{12} and θ_{13} can be obtained simultaneously by introducing a small correction ($\alpha \simeq 0.9997$) in MTM1($A_{12,21}^{(2)}$). Therefore, we only consider the MTM1($A_{12,21}^{(2)}$) hereafter in this study.

Figure 4 presents the predicted values of θ_{13} (upper panel) and θ_{23} (lower panel) as a function of ϕ in the MTM1($A_{12,21}^{(2)}$). The upper, middle, and lower horizontal

Fig. 6. s_{23}^2 vs θ for ϕ [rad] = 0, $\frac{\pi}{4}$, $\frac{\pi}{2}$ in the case of MTM1($A_{12,21}^{(2)}$).

dotted lines represent the 3σ upper limit, the best-fit value, and the 3σ lower limit of θ_{13} (θ_{23}) in the NO case, respectively, in the upper (lower) panel. Fig. 4 indicates that by appropriately selecting ϕ and θ , we can obtain the values of θ_{13} and θ_{23} that are consistent with the observed data. Moreover, we confirmed that s_{13}^2 and s_{23}^2 can be obtained in the 3σ region based on our numerical parameter search.

A benchmark point

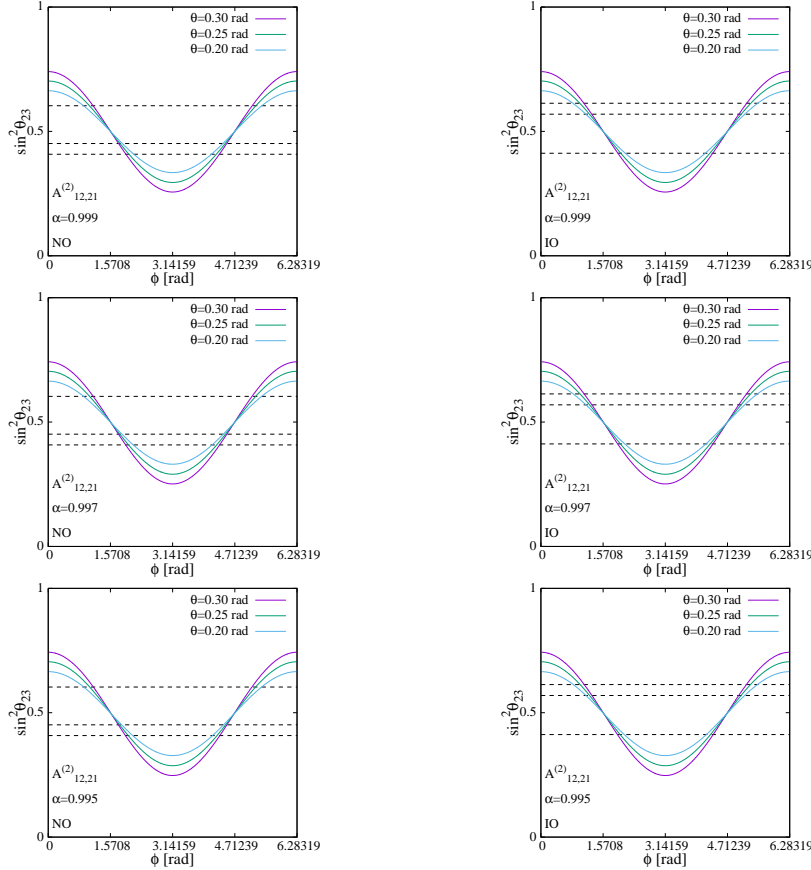
$$(\alpha, \theta, \phi) = (0.99973, 15.50^\circ, 82.56^\circ), \quad (43)$$

yields the best-fit values of s_{12}^2 and s_{13}^2 and the allowed value of s_{23}^2 as follows:

$$(s_{12}^2, s_{23}^2, s_{13}^2, \delta) = (0.303, 0.529, 0.02225, 269.5^\circ). \quad (44)$$

The reader may naturally ask the following issues:

- Q1:** What values should be assigned to the parameters θ , ϕ and α , in order to obtain a reasonable leptonic mixing matrix? Can they be varied in a wide range? Are they correlated?

Fig. 7. s_{23}^2 vs ϕ [rad] = 0.20, 0.25, 0.30 in the case of MTM1($A_{12,21}^{(2)}$).

Q2: What if the values of θ_{23} and the CP phase δ are finally pinned down?

To answer these questions, we show Figures 5 - 9. These figures present the detailed behaviors of the parameters and the predicted values for $\alpha = 0.995, 0.997, 0.999$ in the case of MTM1($A_{12,21}^{(2)}$). The dotted lines in these figures represent the best-fit value (center dotted line) and 3σ region (upper and lower dotted lines) of the physical quantity which is shown in vertical axis. The left-side (right-side) panels in these figures excepted with Figure 5 show the allowed region of the parameters, etc., for NO (IO). The physical quantities compared in these figures are

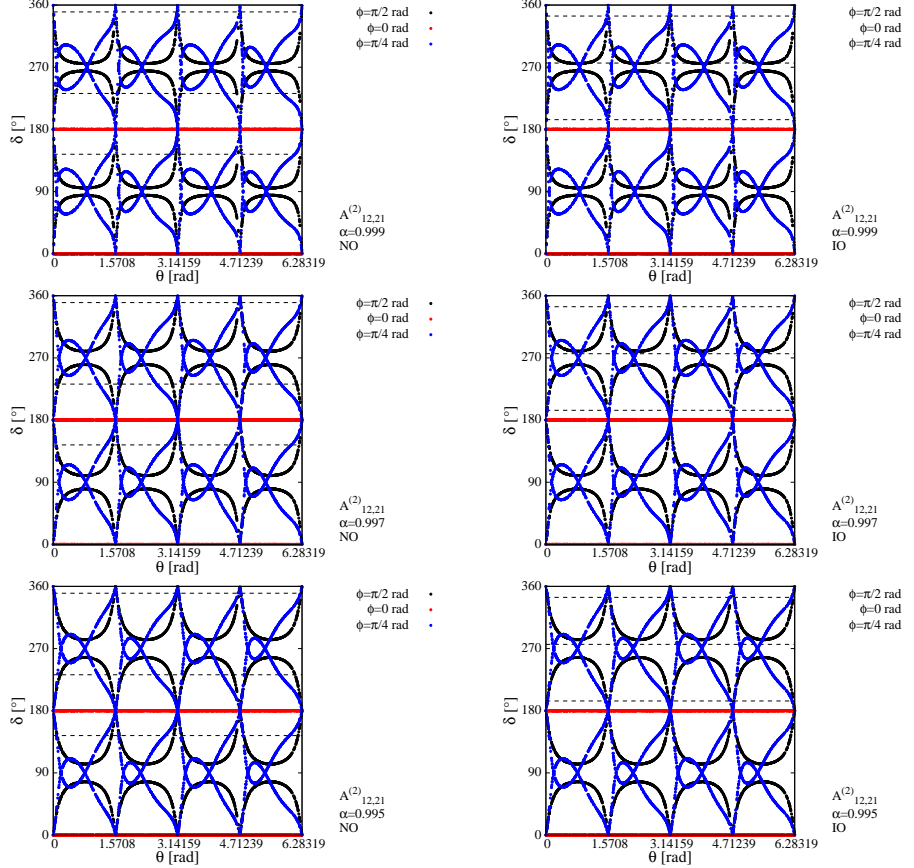
Figure 5: s_{12}^2 (left-side panels) or s_{13}^2 (right-side panels) vs θ for ϕ [rad] = 0, $\frac{\pi}{4}$, $\frac{\pi}{2}$,

Figure 6: s_{23}^2 vs θ for ϕ [rad] = 0, $\frac{\pi}{4}$, $\frac{\pi}{2}$,

Figure 7: s_{23}^2 vs ϕ for θ [rad] = 0.20, 0.25, 0.30,

Figure 8: δ vs θ for ϕ [rad] = 0, $\frac{\pi}{4}$, $\frac{\pi}{2}$,

Figure 9: δ vs ϕ for θ [rad] = 0.20, 0.25, 0.30.

Fig. 8. δ vs θ for ϕ [rad] = 0, $\frac{\pi}{4}$, $\frac{\pi}{2}$ in the case of MTM1($A_{12,21}^{(2)}$).

From these figures, we can conclude that

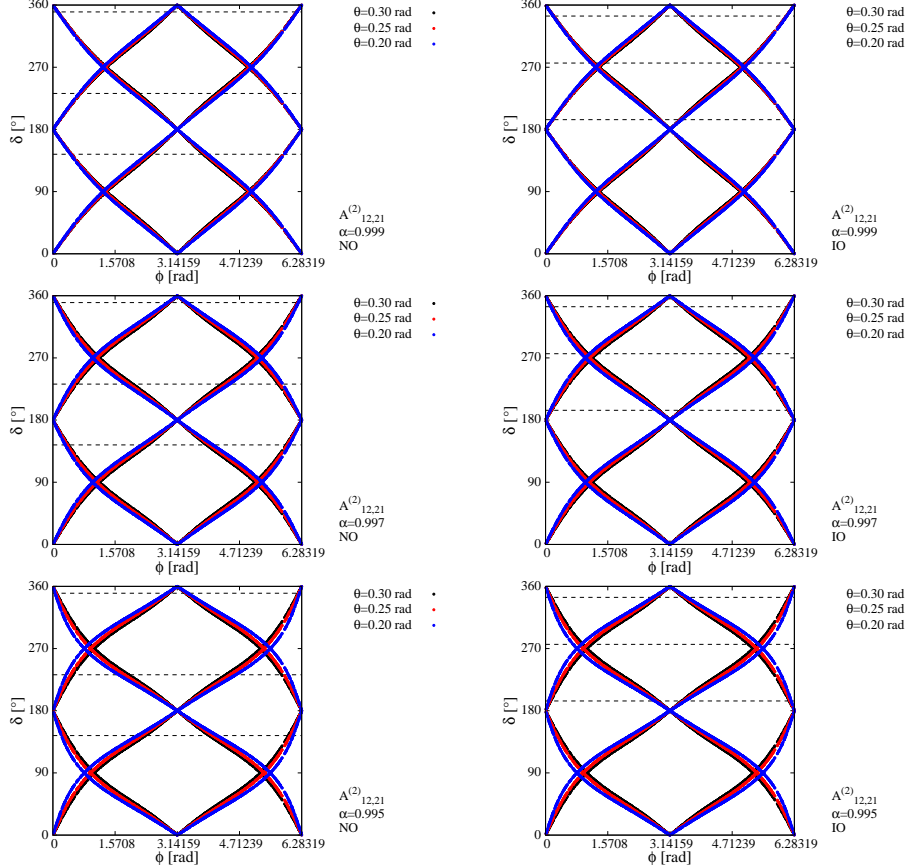
- A1:** The wide range of parameters θ , ϕ and α are consistent with observation (see Figures 5, 6 and 7). The wide range of Dirac CP phase is also consistent with observation (see Figures 8 and 9).
- A2:** If the values of θ_{23} and the CP phase δ are finally pinned down, we can reproduce these fixed values with appropriate values of α , θ and ϕ .

Moreover, the reader may also naturally ask the following question:

- Q3:** What if the best-fit values change in the future?

To answer this critical question, first, we define the ratio

$$R = \frac{s_{12}^2}{s_{13}^2}. \quad (45)$$

Fig. 9. δ vs ϕ for θ [rad] = 0.20, 0.25, 0.30 in the case of MTM1($A_{12,21}^{(2)}$).

The value of R for the current best-fit values is calculated as

$$R_{\text{best-fit}} = 13.618. \quad (46)$$

Then, we show Figure 10. Figure 10 presents the relation between R and α in the case of MTM1($A_{12,21}^{(2)}$) for θ [rad] = 0.22, 0.24, 0.26 (left-side panels) and for ϕ [rad] = 0, $\frac{\pi}{4}$, $\frac{\pi}{2}$ (right-side panels). The dotted lines in the panels represent $R_{\text{best-fit}}$. From Figure 10, it turned out that

A3: if the best-fit values (or equivalently the ratio $R_{\text{best-fit}}$) change in the future, the new best-fit values can be reproduced with appropriate selection of the values of α , θ , ϕ .

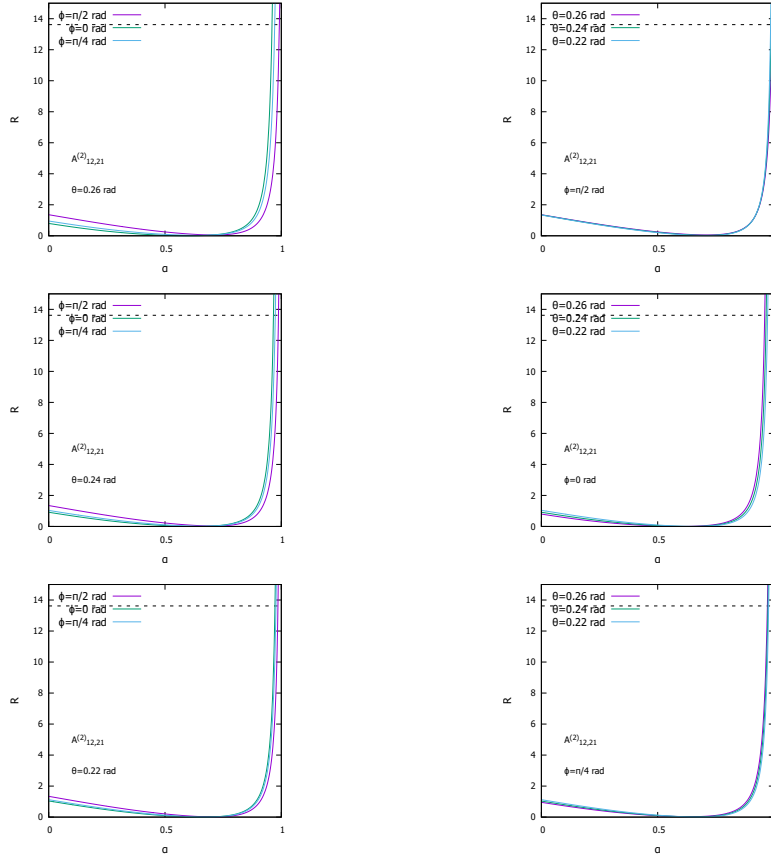


Fig. 10. Relation between R and α in the case of MTM1($A_{12,21}^{(2)}$) for θ [rad] = 0.22, 0.24, 0.26 (left-side panels) and for ϕ [rad] = 0, $\frac{\pi}{4}$, $\frac{\pi}{2}$ (right-side panels).

4.2. $A_{23,32}^{(1)}$ and $A_{23,32}^{(2)}$

We modify TM1 mixing using the rotation matrix $A_{23,32}^{(1)}$ and $A_{23,32}^{(2)}$ as follows:

$$\tilde{U}_1(A_{23,32}^{(1)}) = A_{23,32}^{(1)} U_1, \quad \tilde{U}_1(A_{23,32}^{(2)}) = A_{23,32}^{(2)} U_1, \quad (47)$$

and we call these mixings MTM1($A_{23,32}^{(1)}$) and MTM1($A_{23,32}^{(2)}$), respectively. The mixing angles are

$$s_{12}^2 = \frac{1 - 3s_{13}^2}{3(1 - s_{13}^2)}, \quad (48)$$

$$s_{23}^2 = \frac{1}{12(1 - s_{13}^2)} \left\{ 5 \mp 2\alpha\sqrt{1 - \alpha^2} + (1 \mp 10\alpha\sqrt{1 - \alpha^2}) \cos 2\theta - 2\sqrt{6}(1 - 2\alpha^2) \sin 2\theta \cos \phi \right\},$$

$$s_{13}^2 = \frac{1}{3} \sin^2 \theta. \quad (49)$$

The negative sign of \mp should be taken for MTM1($A_{23,32}^{(1)}$), and the positive sign should be taken for MTM1($A_{23,32}^{(2)}$).

Eq.(48) is equal to Eq.(12). Moreover, Eq.(49) is equal to Eq.(10). Therefore, the simultaneous reproducibility of θ_{12} and θ_{13} is not improved in MTM1($A_{23,32}^{(1)}$) and MTM1($A_{23,32}^{(2)}$). For this reason, no further analysis is performed for MTM1($A_{23,32}^{(1)}$) and MTM1($A_{23,32}^{(2)}$).

4.3. $A_{13,31}^{(1)}$ and $A_{13,31}^{(2)}$

We modify the TM1 mixing scheme using the rotation matrix $A_{13,31}^{(1)}$ and $A_{13,31}^{(2)}$ as follows:

$$\tilde{U}_1(A_{13,31}^{(1)}) = A_{13,31}^{(1)} U_1, \quad \tilde{U}_1(A_{13,31}^{(2)}) = A_{13,31}^{(2)} U_1, \quad (50)$$

and we call these mixings MTM1($A_{13,31}^{(1)}$) and MTM1($A_{13,31}^{(2)}$), respectively. The mixing angles are

$$s_{12}^2 = \frac{5 \pm 4\alpha\sqrt{1 - \alpha^2} - 3\alpha^2 - 6s_{13}^2}{6(1 - s_{13}^2)}, \quad (51)$$

$$s_{23}^2 = \frac{5 + \cos 2\theta + 2\sqrt{6} \sin 2\theta \cos \phi}{12(1 - s_{13}^2)}, \quad (52)$$

$$s_{13}^2 = \frac{1}{6}(3 - 3\alpha^2 - B_1 - B_2). \quad (53)$$

The upper sign of \pm and \mp should be taken for MTM1($A_{13,31}^{(1)}$). The lower sign of these should be taken for MTM1($A_{13,31}^{(2)}$).

Eq.(51) is equal to Eq.(40). Therefore, the simultaneous reproducibility of θ_{12} and θ_{13} in MTM1($A_{13,31}^{(1)}$) and MTM1($A_{13,31}^{(2)}$) is same as MTM1($A_{12,21}^{(1)}$) and MTM1($A_{12,21}^{(2)}$). Thus, the simultaneous reproducibility of θ_{12} and θ_{13} is reduced in MTM1($A_{13,31}^{(1)}$). In contrast, this reproducibility is substantially improved in MTM1($A_{13,31}^{(2)}$). Hereafter, we consider only MTM1($A_{13,31}^{(2)}$).

Figure 11 shows the prediction of θ_{13} (upper panel) and θ_{23} (lower panel) as a function of ϕ in MTM1($A_{13,31}^{(2)}$). Similar to MTM1($A_{12,21}^{(2)}$), Fig. 11 suggests that

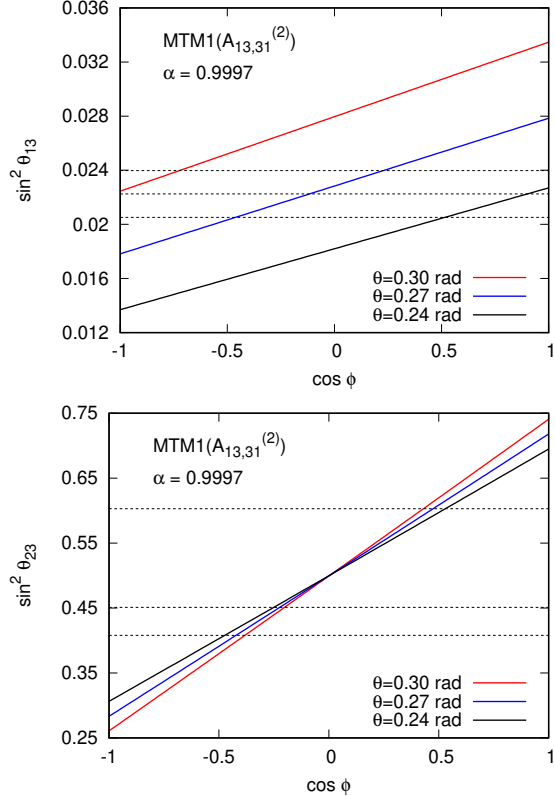


Fig. 11. Same as Fig. 4 but for MTM1($A_{13,31}^{(2)}$).

we can obtain values of θ_{13} and θ_{23} that are consistent with the observations by choosing ϕ and θ . In fact, we have confirmed that s_{13}^2 and s_{23}^2 can be obtained in the 3σ region by numerical parameter search.

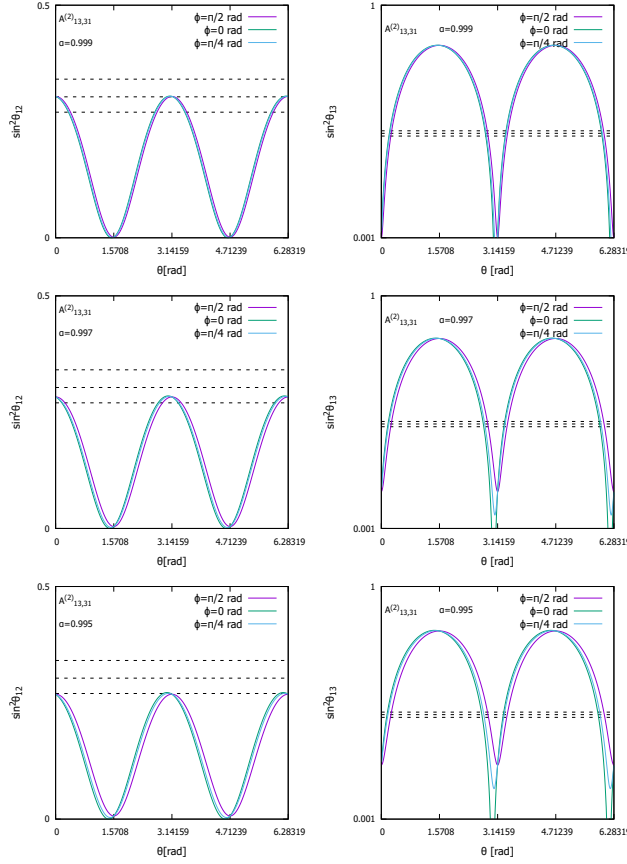
A benchmark point

$$(\alpha, \theta, \phi) = (0.99973, 15.50^\circ, 97.40^\circ), \quad (54)$$

yields the best-fit values of s_{12}^2 and s_{13}^2 simultaneous reproducibility and the allowed value of s_{23}^2 as follows:

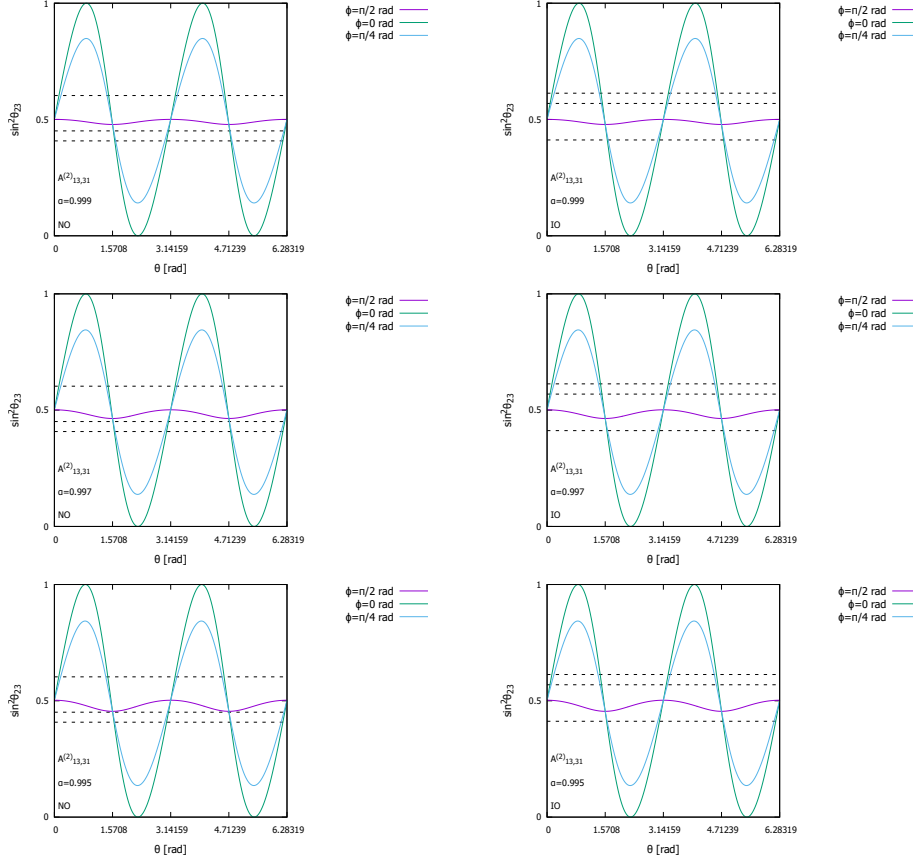
$$(s_{12}^2, s_{23}^2, s_{13}^2, \delta) = (0.303, 0.471, 0.02225, 268.1^\circ). \quad (55)$$

As same as the case of MTM1($A_{12,21}^{(2)}$), the reader may wish to know the ballpark figures of the parameter space and the possible ranges of those mixing parameters in the case of MTM1($A_{13,31}^{(2)}$). Moreover, the reader may wonder what would happen if the best-fit values were changed slightly., or the possible ranges of θ_{23} and δ are narrowed down in the near future.

Fig. 12. Same as Fig. 5 but for MTM1($A_{13,31}^{(2)}$).

To answer these questions, we show Figures 12 - 17. These figures are same as Figures 5 - 10 but for MTM1($A_{13,31}^{(2)}$). From these figures, we have the following similar conclusions for MTM1($A_{13,31}^{(2)}$) as for MTM1($A_{12,21}^{(2)}$),

- The wide range of parameters θ , ϕ and α are consistent with observation (Figures 12, 13 and 14). The wide range of Dirac CP phase is also consistent with observation (Figures 15 and 16).
- If the values of θ_{23} and the CP phase δ are finally pinned down, we can reproduce these fixed values with appropriate values of α , θ and ϕ .
- If the best-fit values change in the future, the new best-fit values can be reproduced with appropriate selection of the values of α , θ , ϕ (Figure 17).

Fig. 13. Same as Fig. 6 but for MTM1($A_{13,31}^{(2)}$)

4.4. Z_2 symmetry breaking

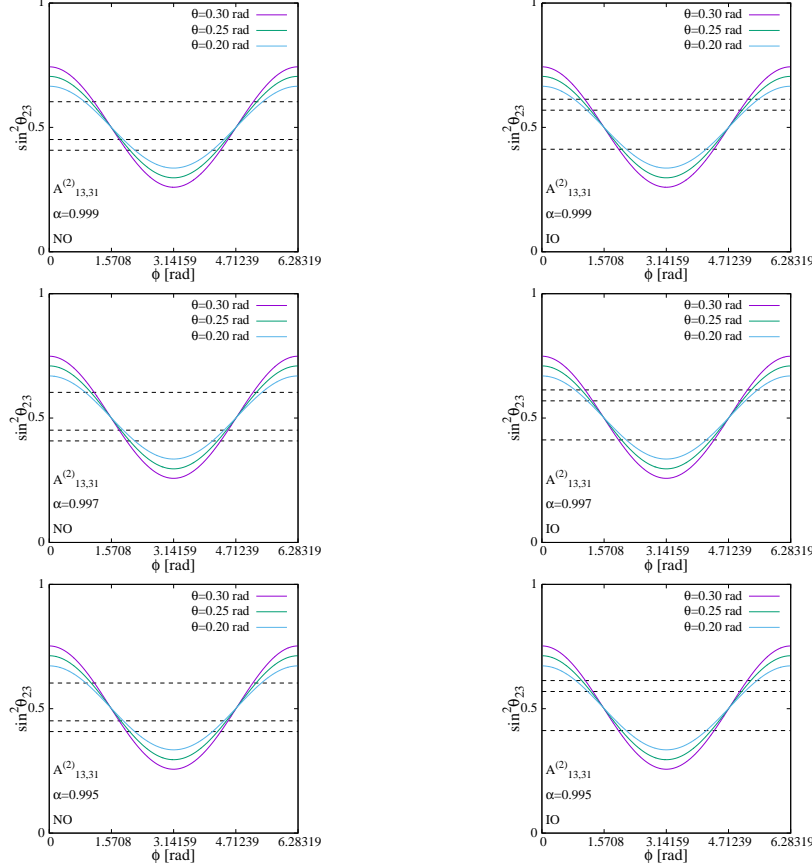
Thus far, it has been found that the modifications of the TM1 mixing using $A_{12,21}^{(2)}$ and $A_{13,31}^{(2)}$ can improve the simultaneous reproducibility of θ_{12} and θ_{13} . However, as a consequence of this improvement, the mass matrix in the modified mixing scheme breaks the Z_2 symmetry, which was strictly preserved in the original TM1 mixing.

The flavor neutrino mass matrix for the modified TM1 mixing with $A = \{A_{12,21}^{(2)}, A_{13,31}^{(2)}\}$ is obtained

$$\tilde{M}_1 = (AU_1)^* D(AU_1)^\dagger = A^* M_1 A^\dagger. \quad (56)$$

The Z_2 transformation of this mass matrix is performed

$$\begin{aligned} S_1 \tilde{M}_1 S_1^T &= S_1 (A^* M_1 A^\dagger) S_1^T \\ &= S_1 A^* (S_1^T S_1) M_1 (S_1^T S_1) A^\dagger S_1^T \\ &= (S_1 A^* S_1^T) M_1 (S_1 A^\dagger S_1^T). \end{aligned} \quad (57)$$

Fig. 14. Same as Fig. 7 but for MTM1($A_{13,31}^{(2)}$)

Using the following definition of δA

$$S_1 A^* S_1^T = A^* + \delta A^*, \quad S_1 A^\dagger S_1^T = A^\dagger + \delta A^\dagger, \quad (58)$$

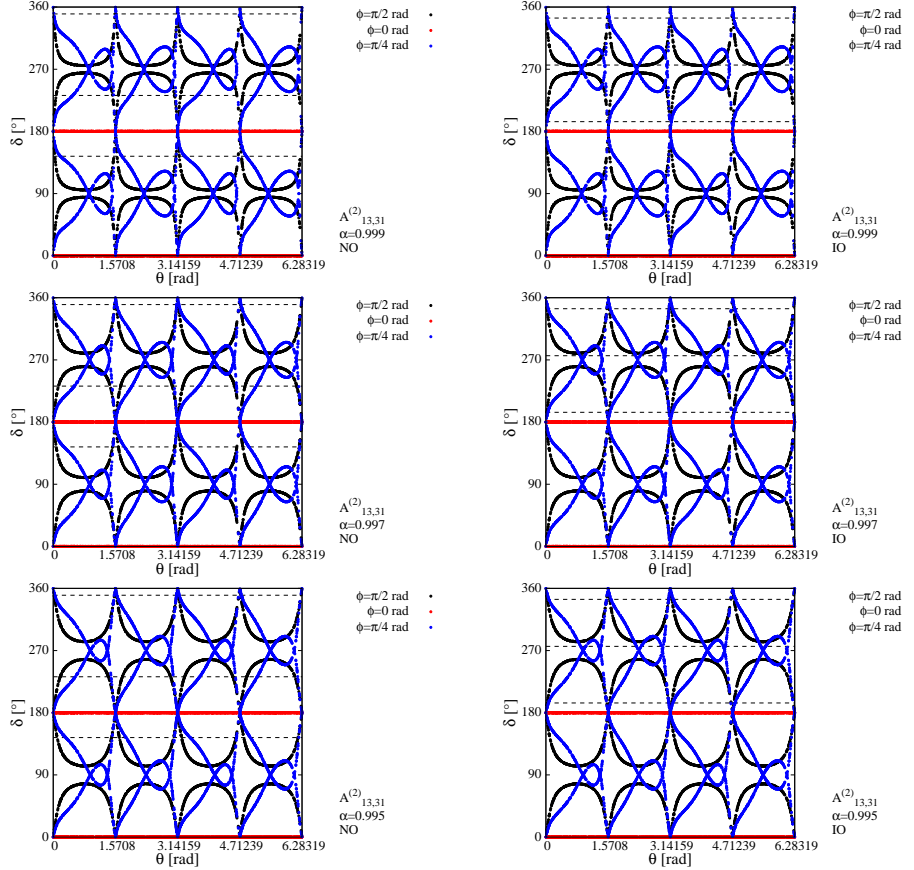
we can write the Z_2 transformation as

$$S_1 \tilde{M}_1 S_1^T = \tilde{M}_1 + \delta \tilde{M}_1, \quad (59)$$

where

$$\begin{aligned} \delta \tilde{M}_1 &= A^* M_1 \delta A^\dagger + \delta A^* M_1 A^\dagger + \delta A^* M_1 \delta A^\dagger \\ &= A^* M_1 (A^\dagger A) \delta A^\dagger + \delta A^* (A^T A^*) M_1 A^\dagger + \delta A^* (A^T A^*) M_1 (A^\dagger A) \delta A^\dagger \quad (60) \\ &= \tilde{M}_1 A \delta A^\dagger + (A \delta A^\dagger)^T \tilde{M}_1 + (A \delta A^\dagger)^T \tilde{M}_1 A \delta A^\dagger. \end{aligned}$$

The magnitude of the symmetry breaking of Z_2 can be evaluated by the following

Fig. 15. Same as Fig. 8 but for MTM1($A_{13,31}^{(2)}$)

matrix:

$$\delta_{Z2}^{\text{MTM1}} = \begin{pmatrix} \delta_{11} & \delta_{12} & \delta_{13} \\ * & \delta_{22} & \delta_{23} \\ * & * & \delta_{33} \end{pmatrix}, \quad (61)$$

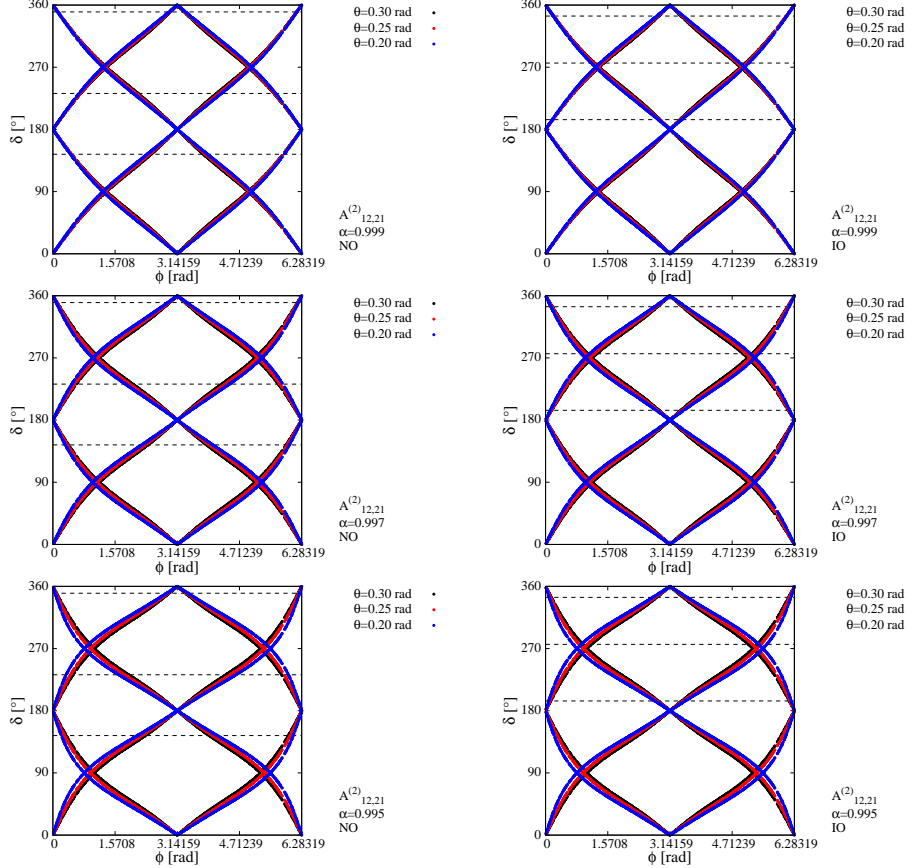
where

$$\delta_{ij} = \frac{|(\tilde{M}_1)_{ij}|}{|(\tilde{M}_1)_{ij}|}, \quad (62)$$

and $*$ indicates the symmetric elements.

For MTM1($A_{12,21}^{(2)}$), the magnitude of Z_2 symmetry breaking at the benchmark point shown in Eq.(43) is obtained as follows:

$$\delta_{Z2}^{\text{MTM1}}(A_{12,21}^{(2)}) = \begin{pmatrix} 0.132 & 0.116 & 0.169 \\ * & 0.0304 & 0.00878 \\ * & * & 0.0452 \end{pmatrix}, \quad (63)$$

Fig. 16. Same as Fig. 9 but for MTM1($A_{13,31}^{(2)}$)

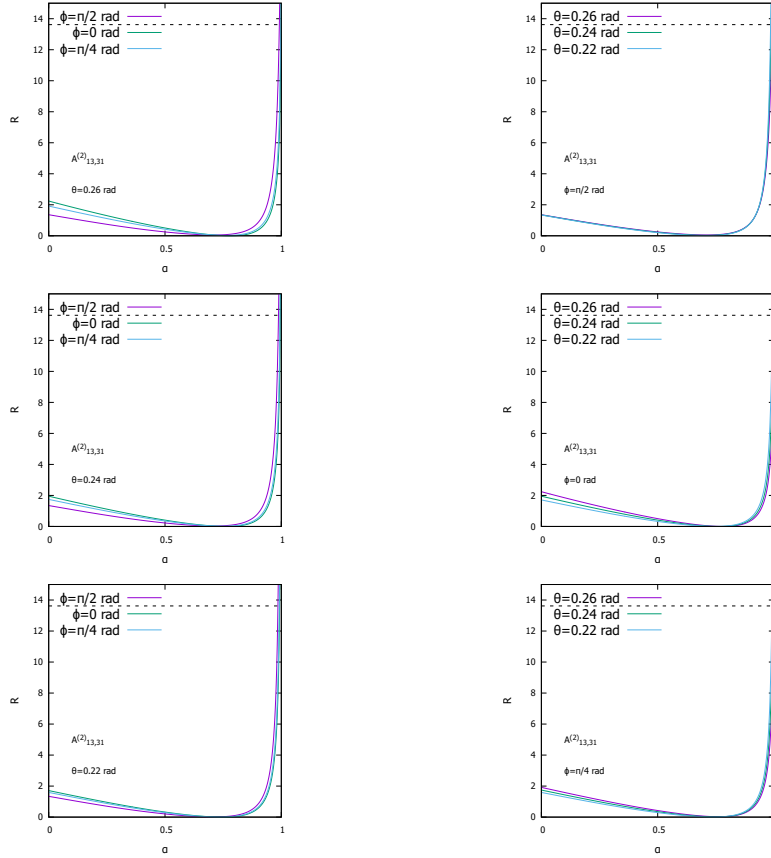
where $(m_1, m_2, m_3) = (0, \Delta m_{21}^2, \Delta m_{31}^2)$ with the best-fit values of Δm_{ij}^2 in NO. The Z_2 symmetry breaking in the first row (maximum 16.9%) is larger than that in the second and third rows (maximum 4.5%). Unfavorably, the magnitude of the symmetry breaking of Z_2 is not small in the electron flavor sector.

Similarly, for MTM1($A_{13,31}^{(2)}$), the magnitude of the symmetry breaking of Z_2 at the benchmark point shown in Eq.(54) is obtained as follows:

$$\delta_{Z2}^{\text{MTM1}}(A_{13,31}^{(2)}) = \begin{pmatrix} 0.133 & 0.171 & 0.117 \\ * & 0.0456 & 0.00880 \\ * & * & 0.0307 \end{pmatrix}. \quad (64)$$

The symmetry breaking of Z_2 in the first row (maximum 17.1%) is larger than that in the second and third rows (maximum 4.6%). Again, the magnitude of the symmetry breaking of Z_2 is not small in the electron flavor sector.

While the theoretical origin of the Z_2 symmetry breaking in the MTM1($A_{12,21}^{(2)}$) and MTM1($A_{13,31}^{(2)}$) mixings is a critical consideration, it is acknowledged that the

Fig. 17. Same as Fig. 10 but for MTM1($A_{13,31}^{(2)}$)

primary focus of this study is to improve the simultaneous reproducibility of θ_{12} and θ_{13} . Therefore, for the purposes of this study, the problem of Z_2 symmetry breaking will be disregarded.

5. Modified TM2 mixing

5.1. $A_{12,21}^{(1)}$ and $A_{12,21}^{(2)}$

The TM2 mixing can also be subject to the same modification method employed for the TM1 mixing. The modified TM2 mixing, utilizing the rotation matrices $A_{12,21}^{(1)}$ and $A_{12,21}^{(2)}$, can be expressed as follows:

$$\tilde{U}_2(A_{12,21}^{(1)}) = A_{12,21}^{(1)} U_2, \quad \tilde{U}_2(A_{12,21}^{(2)}) = A_{12,21}^{(2)} U_2. \quad (65)$$

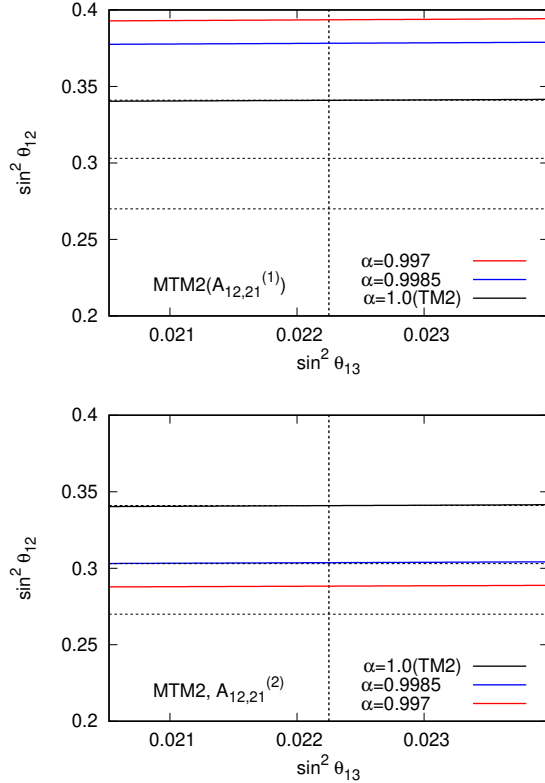


Fig. 18. Same as Fig. 3 but for MTM2.

We call these mixings $\text{MTM2}(A_{12,21}^{(1)})$ and $\text{MTM2}(A_{12,21}^{(2)})$, respectively. The mixing angles are

$$s_{12}^2 = \frac{1 \pm 2\alpha\sqrt{1-\alpha^2}}{3(1-s_{13}^2)}, \quad (66)$$

$$\begin{aligned} s_{23}^2 &= \frac{1}{6(1-s_{13}^2)} \left\{ 3\alpha^2 + (4 - 6\alpha^2 \pm 4\alpha\sqrt{1-\alpha^2}) \sin^2 \theta \right. \\ &\quad \left. + \sqrt{3}\alpha(\alpha \pm 2\sqrt{1-\alpha^2}) \sin 2\theta \cos \phi \right\}, \end{aligned}$$

$$s_{13}^2 = \frac{1}{6}(2 \mp 2\alpha\sqrt{1-\alpha^2} + B_3 + B_4), \quad (67)$$

where

$$\begin{aligned} B_3 &= (1 - 3\alpha^2 \pm 2\alpha\sqrt{1-\alpha^2}) \cos 2\theta, \\ B_4 &= \sqrt{3}(1 - \alpha^2 \mp 2\alpha\sqrt{1-\alpha^2}) \sin 2\theta \cos \phi. \end{aligned} \quad (68)$$

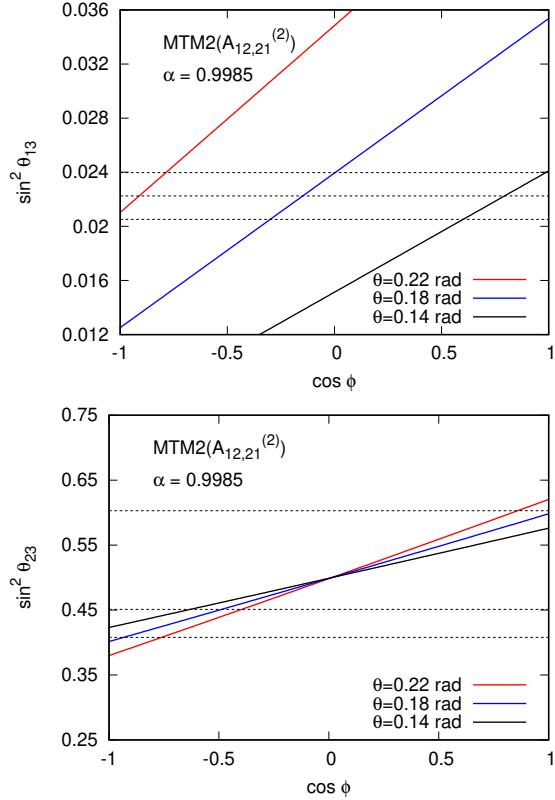
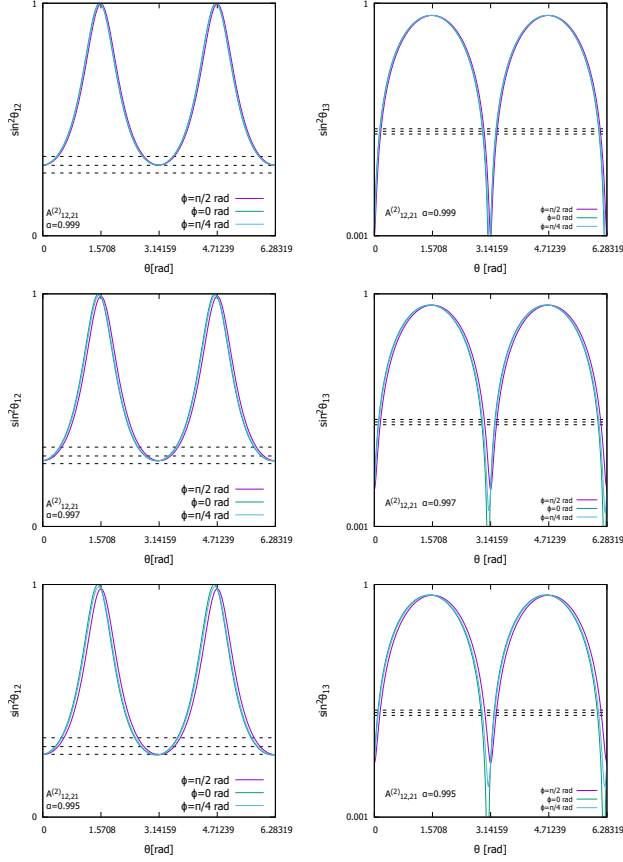


Fig. 19. Same as Fig. 4 but for MTM2.

The upper sign of \pm and \mp should be taken for MTM2($A_{12,21}^{(1)}$). The lower sign of these should be taken for MTM2($A_{12,21}^{(2)}$).

Figure 18 presents the predictions of θ_{13} and θ_{12} in the MTM2($A_{12,21}^{(1)}$) and MTM2($A_{12,21}^{(2)}$) scenarios. The horizontal and vertical dotted lines in each panel correspond to those in Figure 3. Similar to MTM1($A_{12,21}^{(1)}$) and MTM1($A_{12,21}^{(2)}$), the simultaneous reproducibility of θ_{12} and θ_{13} is reduced in MTM2($A_{12,21}^{(1)}$). Conversely, this reproducibility is significantly improved in MTM2($A_{12,21}^{(2)}$). For instance, the best-fit values of θ_{12} and θ_{13} can be obtained simultaneously with a small correction ($\alpha \simeq 0.9985$). Moving forward, we will solely focus on MTM2($A_{12,21}^{(2)}$).

Figure 19 illustrates the prediction of θ_{13} (upper panel) and θ_{23} (lower panel) as a function of ϕ in the MTM2($A_{12,21}^{(2)}$) scenario. Similar to MTM1($A_{12,21}^{(2)}$), the figure suggests that by selecting appropriate values of ϕ and θ , we can obtain θ_{13} and θ_{23} values that are consistent with the observations. Through our numerical parameter search, we have confirmed that s_{13}^2 and s_{23}^2 can be obtained within the 3σ region.

Fig. 20. Same as Fig. 5 but for MTM2($A_{12,21}^{(2)}$).

A benchmark point

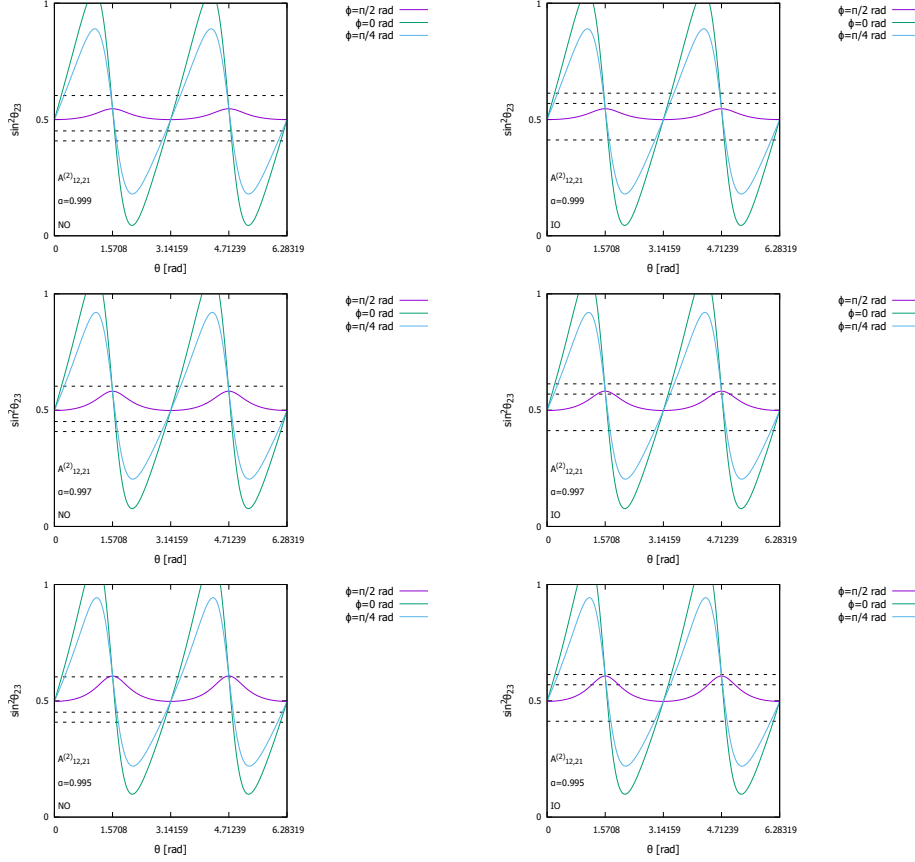
$$(\alpha, \theta, \phi) = (0.99847, 10.31^\circ, 98.61^\circ), \quad (69)$$

yields the best-fit values of s_{12}^2 and s_{13}^2 and the allowed value of s_{23}^2 as follows:

$$(s_{12}^2, s_{23}^2, s_{13}^2, \delta) = (0.303, 0.484, 0.02225, 263.8^\circ). \quad (70)$$

Figures 20 - 25 show that the ballpark figures of the parameter space and the possible ranges of those mixing parameters. From these figures, we have the similar conclusions for MTM2($A_{12,21}^{(2)}$) as for MTM1($A_{12,21}^{(2)}$) as follows,

- The wide range of parameters θ , ϕ and α are consistent with observations (Figures 20, 21 and 22). The wide range of Dirac CP phase is also consistent with observation (Figures 23 and 24).
- If the values of θ_{23} and the CP phase δ are finally pinned down, we can reproduce these fixed values with appropriate values of α , θ and ϕ .

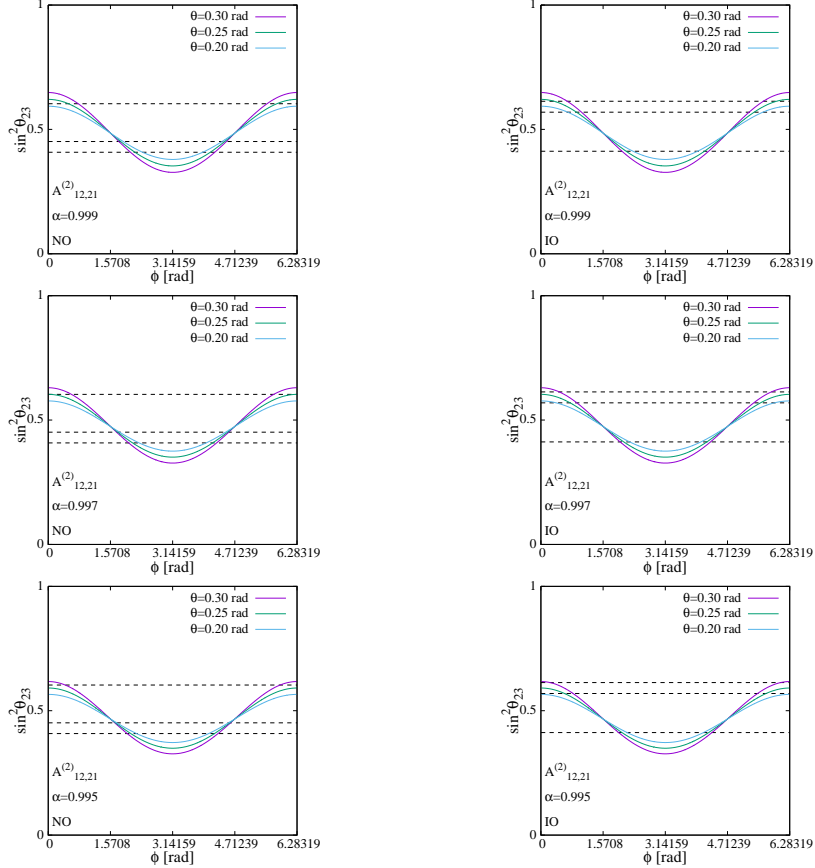
Fig. 21. Same as Fig. 6 but for MTM2($A_{12,21}^{(2)}$)

- If the best-fit values change in the future, the new best-fit values can be reproduced with appropriate selection of the values of α , θ , ϕ (Figure 25).

5.2. $A_{23,32}^{(1)}$ and $A_{23,32}^{(2)}$

We modify TM2 mixing using the rotation matrix $A_{23,32}^{(1)}$ and $A_{23,32}^{(2)}$ as follows:

$$\tilde{U}_2(A_{23,32}^{(1)}) = A_{23,32}^{(1)} U_2, \quad \tilde{U}_2(A_{23,32}^{(2)}) = A_{23,32}^{(2)} U_2, \quad (71)$$

Fig. 22. Same as Fig. 7 but for MTM2($A_{12,21}^{(2)}$)

and we call these mixings MTM2($A_{23,32}^{(1)}$) and MTM2($A_{23,32}^{(2)}$), respectively. The mixing angles are

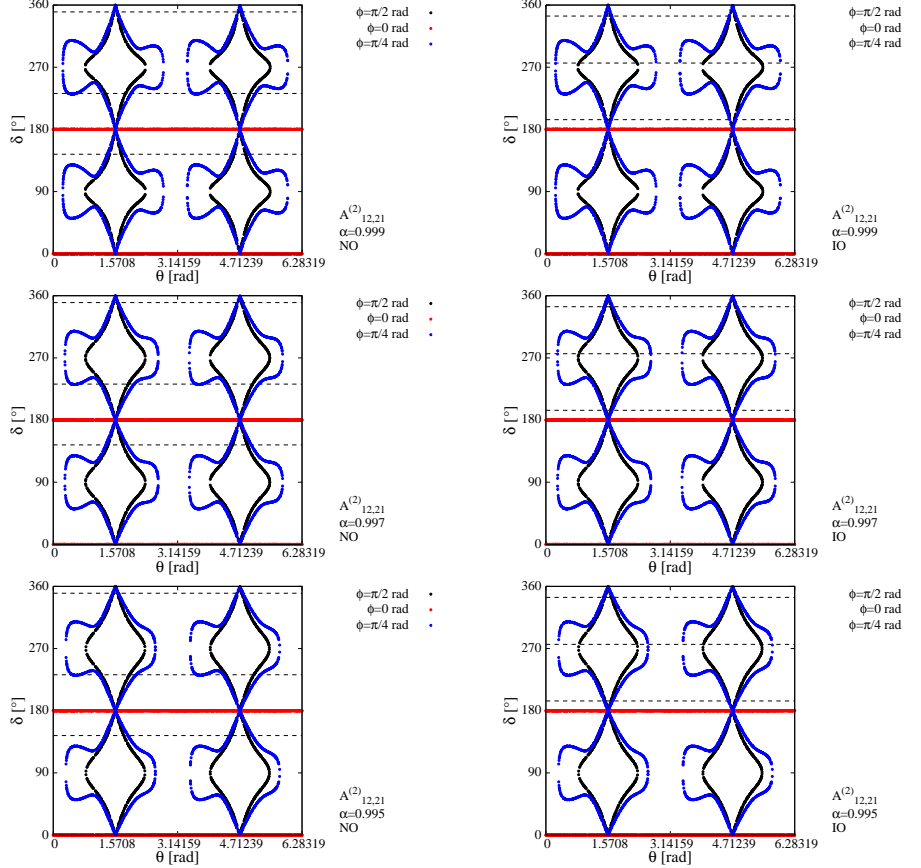
$$s_{12}^2 = \frac{1}{3(1 - s_{13}^2)}, \quad (72)$$

$$\begin{aligned} s_{23}^2 &= \frac{1}{6(1 - s_{13}^2)} \left\{ 2 \mp 2\alpha\sqrt{1 - \alpha^2} + (1 \mp 4\alpha\sqrt{1 - \alpha^2} \cos 2\theta \right. \\ &\quad \left. + \sqrt{3}(2\alpha^2 - 1) \sin 2\theta \cos \phi) \right\}. \end{aligned}$$

$$s_{13}^2 = \frac{2}{3} \sin^2 \theta. \quad (73)$$

The negative sign of \mp should be taken for MTM2($A_{23,32}^{(1)}$), and the positive sign should be taken for MTM2($A_{23,32}^{(2)}$).

After comparing Eq. (72) and Eq. (20), as well as Eq. (73) and Eq. (18), it is evident that the simultaneous reproducibility of θ_{12} and θ_{13} is not improved in

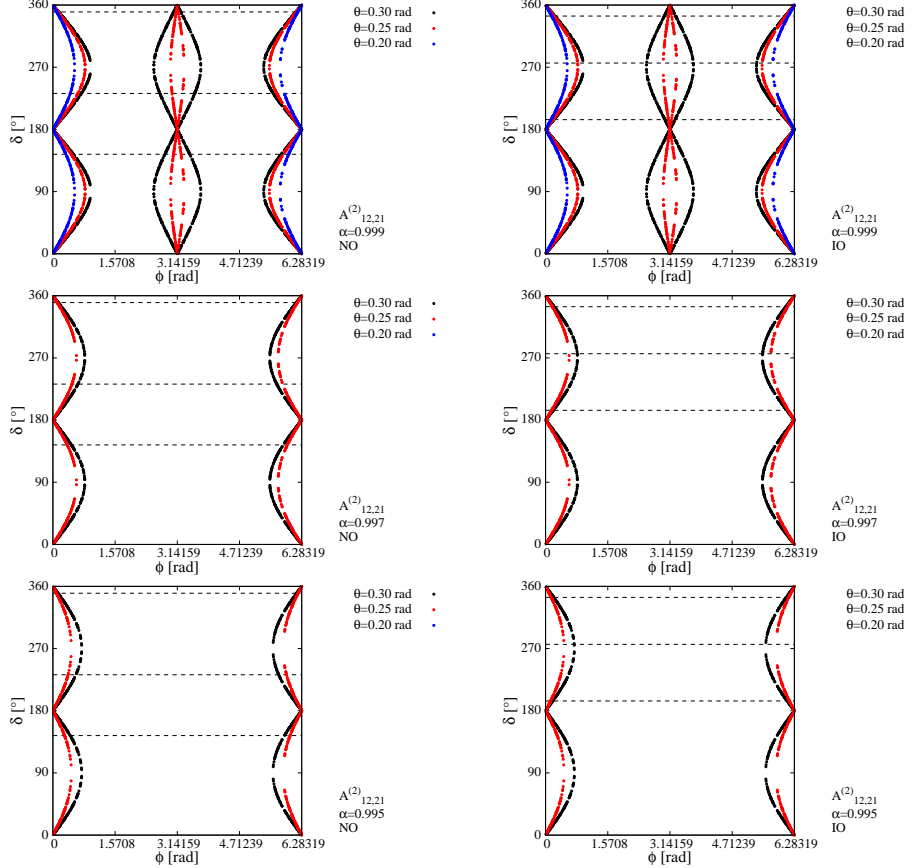
Fig. 23. Same as Fig. 8 but for MTM2($A_{12,21}^{(2)}$)

MTM2($A_{23,32}^{(1)}$) and MTM2($A_{23,32}^{(2)}$). Therefore, no further analysis is conducted for MTM2($A_{23,32}^{(1)}$) and MTM2($A_{23,32}^{(2)}$).

5.3. $A_{13,31}^{(1)}$ and $A_{13,31}^{(2)}$

The modified TM2 mixing scheme involving the rotation matrices $A_{13,31}^{(1)}$ and $A_{13,31}^{(2)}$ is obtained as follows:

$$\tilde{U}_2(A_{13,31}^{(1)}) = A_{13,31}^{(1)} U_2, \quad \tilde{U}_2(A_{13,31}^{(2)}) = A_{13,31}^{(2)} U_2, \quad (74)$$

Fig. 24. Same as Fig. 9 but for MTM2($A_{12,21}^{(2)}$).

and we term these mixing schemes as MTM2($A_{13,31}^{(1)}$) and MTM2($A_{13,31}^{(2)}$), respectively. The mixing angles are

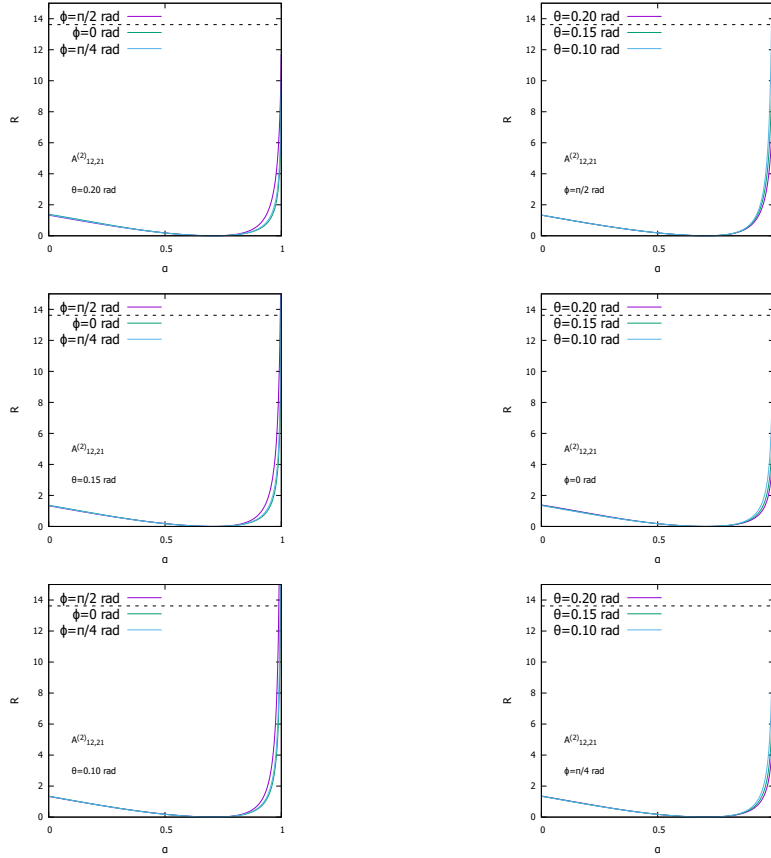
$$s_{12}^2 = \frac{1 \pm 2\alpha\sqrt{1-\alpha^2}}{3(1-s_{13}^2)}, \quad (75)$$

$$s_{23}^2 = \frac{2 + \cos 2\theta + \sqrt{3} \sin 2\theta \cos \phi}{6(1-s_{13}^2)}, \quad (76)$$

$$s_{13}^2 = \frac{1}{6}(2 \mp 2\alpha\sqrt{1-\alpha^2} + B_3 - B_4). \quad (77)$$

The upper sign of \pm and \mp must be considered in case of the MTM2($A_{13,31}^{(1)}$), and the lower sign of \pm and \mp must be considered in case of the MTM2($A_{13,31}^{(2)}$).

Eq.(75) is equal to Eq.(66). Thus, the simultaneous reproducibility of θ_{12} and θ_{13} is diminished using the MTM2($A_{13,31}^{(1)}$). By contrast, the simultaneous reproducibility of θ_{12} and θ_{13} is substantially enhanced using the MTM2($A_{13,31}^{(2)}$). Therefore, we

Fig. 25. Same as Fig. 10 but for MTM2($A_{12,21}^{(2)}$).

only consider the MTM2($A_{13,31}^{(2)}$) for analyses in this study.

Figure 26 depicts the predicted values of θ_{13} (upper panel) and θ_{23} (lower panel) with respect to ϕ based on the MTM2($A_{13,31}^{(2)}$). Similar to the results obtained using the MTM2($A_{12,21}^{(2)}$), Fig. 26 indicates that the values of θ_{13} and θ_{23} that are consistent with the observed data can be obtained by choosing the appropriate values of ϕ and θ . We confirmed this result based on our numerical parameter search.

A benchmark point

$$(\alpha, \theta, \phi) = (0.99847, 10.31^\circ, 81.41^\circ), \quad (78)$$

yields the best-fit values of s_{12}^2 and s_{13}^2 and the allowed value of s_{23}^2 as follows:

$$(s_{12}^2, s_{23}^2, s_{13}^2, \delta) = (0.303, 0.514, 0.02225, 262.3^\circ). \quad (79)$$

Figures 27 - 32 show that the ballpark figures of the parameter space and the

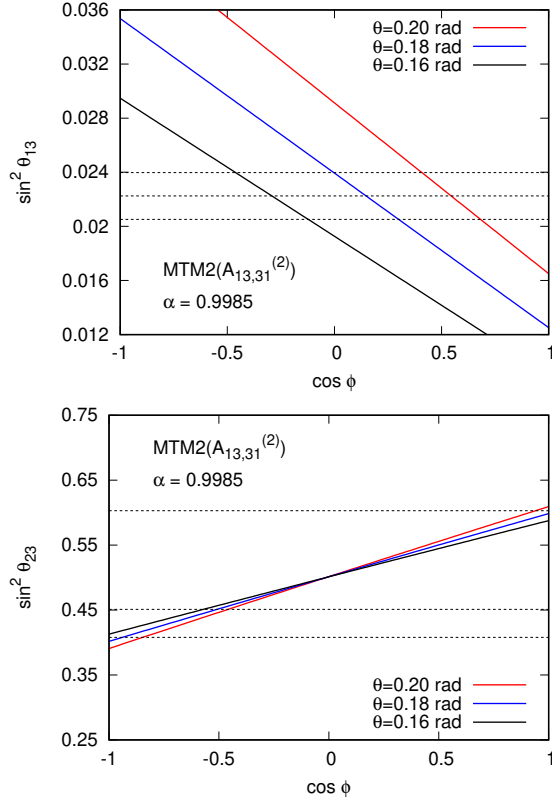


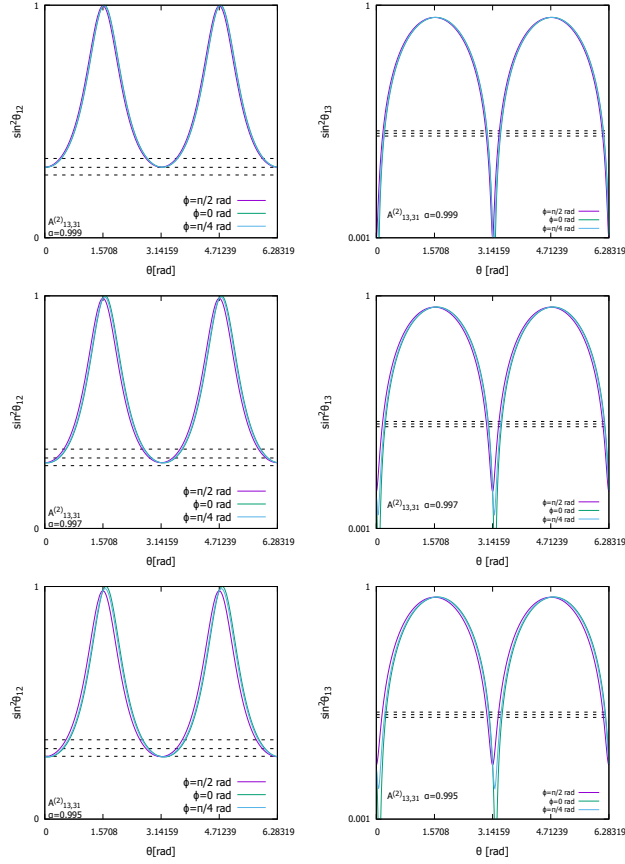
Fig. 26. Same as Fig. 4 but for MTM2.

possible ranges of those mixing parameters. From these figures, we have the similar conclusions for MTM2($A_{13,31}^{(2)}$) as for MTM1($A_{13,31}^{(2)}$) as follows,

- The wide range of parameters θ , ϕ and α are allowed with observations (Figures 27, 28 and 29). The wide range of Dirac CP phase is also consistent with observation (Figures 30 and 31).
- If the values of θ_{23} and the CP phase δ are finally pinned down, we can reproduce these fixed values with appropriate values of α , θ and ϕ .
- If the best-fit values change in the future, the new best-fit values can be reproduced with appropriate selection of the values of α , θ , ϕ (Figure 32).

5.4. Z_2 symmetry breaking

Similar to the results of modification introduced in the TM1 mixing scheme, modifications to the TM2 mixing scheme realized via the introduction of $A_{12,21}^{(2)}$ and $A_{13,31}^{(2)}$ can improve the simultaneous reproducibility of θ_{12} and θ_{13} . However, the Z_2 symmetry related to the mass matrices is broken owing to the modifications

Fig. 27. Same as Fig. 5 but for MTM2($A_{13,31}^{(2)}$).

introduced the mixing scheme.

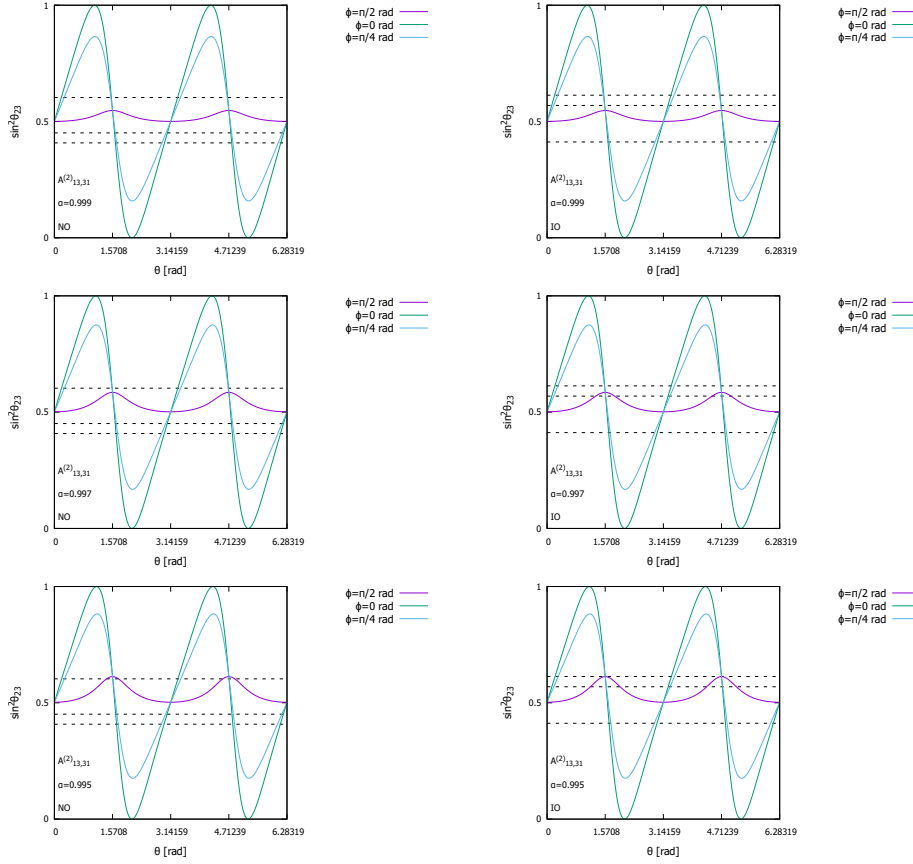
With respect to the MTM2($A_{12,21}^{(2)}$), the magnitude of Z_2 symmetry breaking at the benchmark point shown in Eq.(69) can be determined as follows:

$$\delta_{Z2}^{\text{MTM2}}(A_{12,21}^{(2)}) = \begin{pmatrix} 0.211 & 0.139 & 0.267 \\ * & 0.1201 & 0.0137 \\ * & * & 0.0804 \end{pmatrix}, \quad (80)$$

where $(m_1, m_2, m_3) = (0, \Delta m_{21}^2, \Delta m_{31}^2)$ with the best-fit values of Δm_{ij}^2 in the case of NO.

Similarly, for MTM2($A_{13,31}^{(2)}$), the magnitude of Z_2 symmetry breaking at the benchmark point shown in Eq.(78) can be determined as follows:

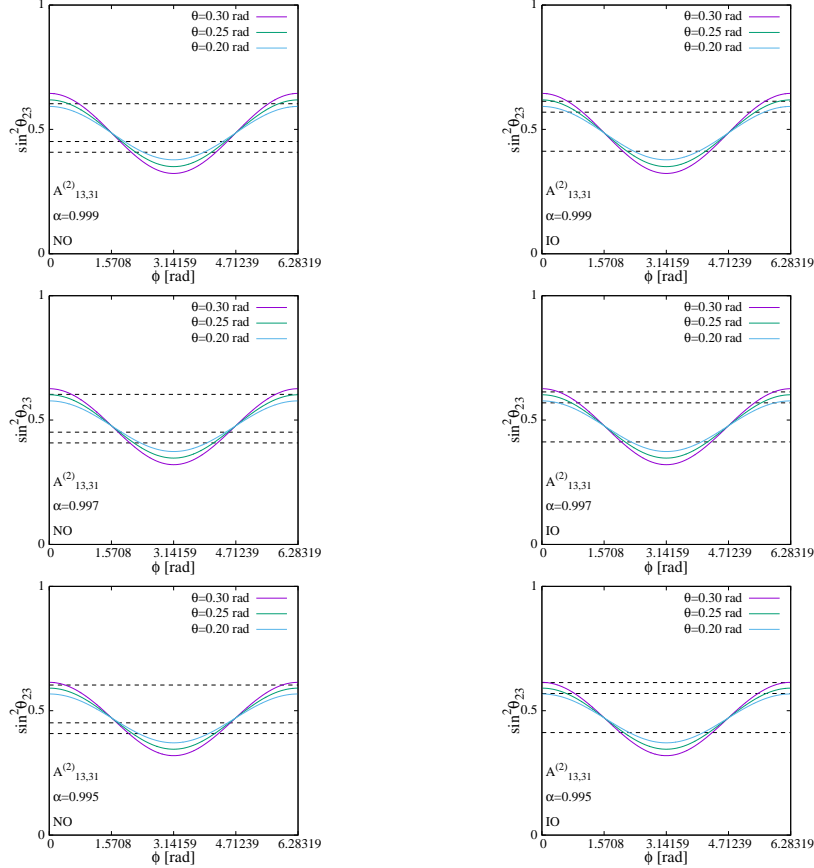
$$\delta_{Z2}^{\text{MTM1}}(A_{13,31}^{(2)}) = \begin{pmatrix} 0.208 & 0.261 & 0.134 \\ * & 0.0775 & 0.0136 \\ * & * & 0.116 \end{pmatrix}. \quad (81)$$

Fig. 28. Same as Fig. 6 but for MTM2($A_{13,31}^{(2)}$)

The magnitude of maximum Z_2 symmetry breaking with respect to the MTM1($A_{12,21}^{(2)}$) and MTM1($A_{13,31}^{(2)}$) is 17%, while the magnitude of maximum Z_2 symmetry breaking with respect to the MTM2($A_{12,21}^{(2)}$) and MTM2($A_{13,31}^{(2)}$) is 27%. This is because the simultaneous reproducibility of θ_{12} and θ_{13} in the original TM1 scheme is larger than that in the original TM2 scheme. Hence, substantial modifications are necessary in the TM2 scheme to achieve the desired level of reproducibility.

6. Summary

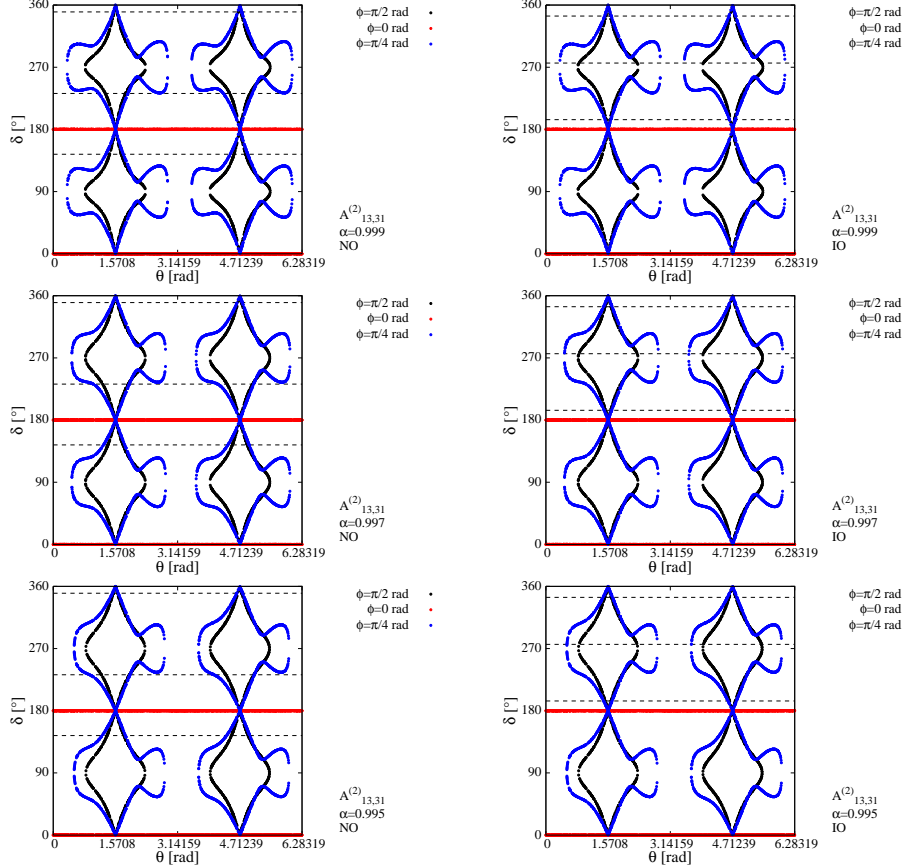
The two types of trimaximal mixing schemes, TM1 and TM2, are widely studied neutrino mixing schemes. The values of neutrino mixing angles predicted using TM1 and TM2 are consistent with the experimentally observed data. However, TM1 and TM2 cannot simultaneously predict the best-fit values of θ_{12} and θ_{13} . Specifically, in the case of TM2, the predicted value of θ_{12} approaches the upper limit of the 3σ allowed region. Hence, the TM2 mixing scheme may soon be excluded from neutrino

Fig. 29. Same as Fig. 7 but for MTM2($A_{13,31}^{(2)}$)

oscillation experiments.

Although simultaneous reproducibility of θ_{12} and θ_{13} cannot be realized using the TM1 and TM2 mixing schemes, these schemes are still widely studied because the flavor neutrino mass matrices in the TM1 and TM2 mixing schemes are invariant under the exact Z_2 symmetry. We have attempted to develop modified versions of the TM1 and TM2 mixing schemes that could maintain the exact Z_2 symmetry; however, these attempts have not yet been successful. In this study, we developed modified TM1 and TM2 mixing schemes that involve a certain degree of Z_2 symmetry breaking to realize the desired simultaneous reproducibility.

We observed that unitarity of the modified mixing matrix \tilde{U} could be maintained by modifying the original mixing matrix U using $\tilde{U} = AU$, where A has only one real

Fig. 30. Same as Fig. 8 but for MTM2($A_{13,31}^{(2)}$).

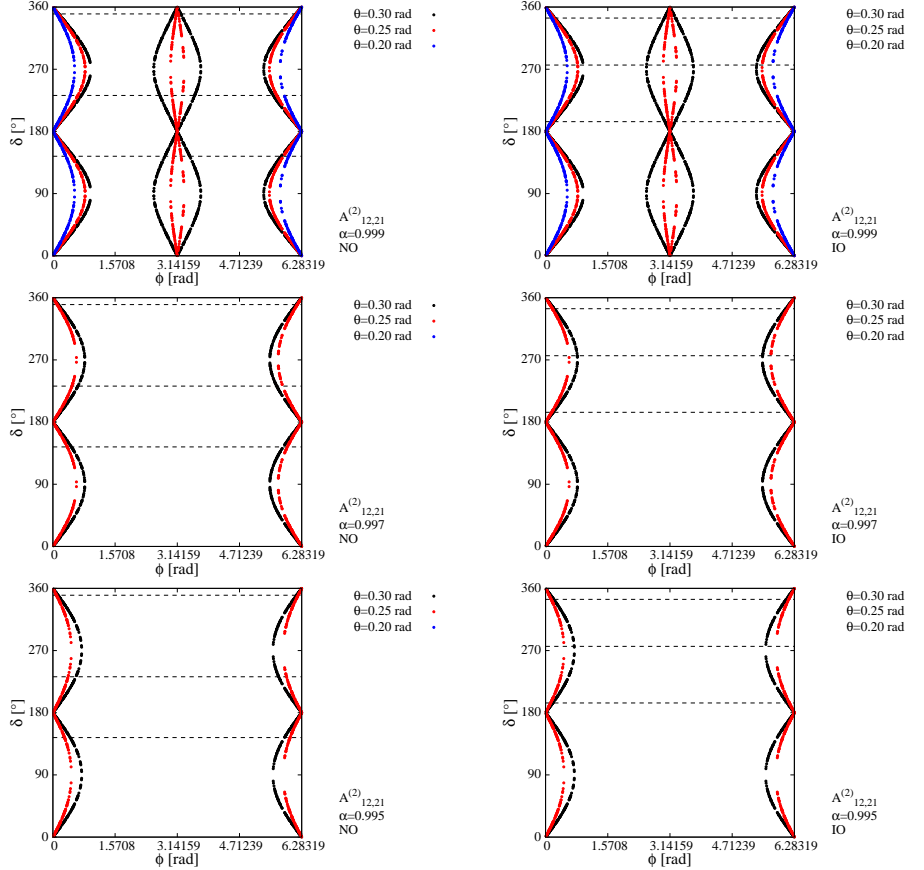
parameter. The two successful modification are based on the following two matrices

$$A_{12,21}^{(2)} = \begin{pmatrix} \alpha & -\sqrt{1-\alpha^2} & 0 \\ \sqrt{1-\alpha^2} & \alpha & 0 \\ 0 & 0 & 1 \end{pmatrix}, \quad (82)$$

and

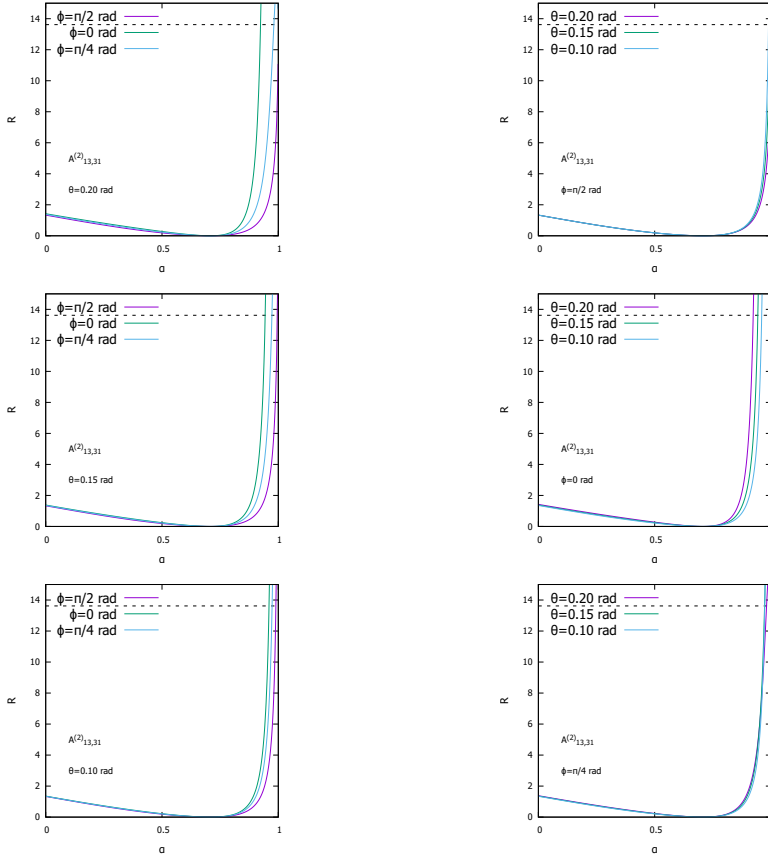
$$A_{13,31}^{(2)} = \begin{pmatrix} \alpha & 0 & -\sqrt{1-\alpha^2} \\ 0 & 1 & 0 \\ \sqrt{1-\alpha^2} & 0 & \alpha \end{pmatrix}, \quad (83)$$

where α denotes the real parameter. We have shown that the modified TM1 and TM2 mixing matrices can simultaneously predict the best-fit values of θ_{12} and θ_{13} using $A_{12,21}^{(2)}$, with $\alpha = 0.99973$, and $A_{13,31}^{(2)}$, with $\alpha = 0.99847$.

Fig. 31. Same as Fig. 9 but for MTM2($A_{13,31}^{(2)}$).

References

1. P. F. Harrison, D. H. Perkins, and W. G. Scott, Phys. Lett. B **530**, 167 (2002).
2. Z. Z. Xing, Phys. Lett. B **533**, 85 (2002).
3. P. F. Harrison and W. G. Scott, Phys. Lett. B **535**, 163 (2002).
4. T. Kitabayashi, Phys. Rev. D **76**, 033002 (2007).
5. M. S. Berger and K. Siyeon, Phys. Rev. D **64**, 053006 (2001).
6. P. H. Frampton, S. L. Glashow, and D. Marfatia, Phys. Lett. B **536**, 79 (2002).
7. Z. Z. Xing, Phys. Lett. B **530**, 159 (2002).
8. Z. Z. Xing, Phys. Lett. B **539**, 85 (2002).
9. A. Kageyama, S. Kaneko, N. Shimoyana, and M. Tanimoto, Phys. Lett. B **538**, 96 (2002).
10. Z. Z. Xing, Phys. Rev. D **69**, 013006 (2004).
11. W. Grimus, A. S. Joshipura, L. Lavoura, and M. Tanimoto, Eur. Phys. J. C **36**, 227 (2004).
12. C. I. Low, Phys. Rev. D **70**, 073013 (2004).
13. C. I. Low, Phys. Rev. D **71**, 073007 (2005).
14. W. Grimus and L. Lavoura, J. Phys. G **31**, 693 (2005).

Fig. 32. Same as Fig. 10 but for MTM2($A_{13,31}^{(2)}$).

15. S. Dev, S. Kumar, S. Verma, and S. Gupta, Phys. Rev. D **76**, 013002 (2007).
16. Z. Z. Xing and S. Zhou, Phys. Lett. B **679**, 249 (2009).
17. H. Fritzsch, Z. Z. Xing, and S. Zhou, J. High Energy Phys. **09**, 083 (2011).
18. S. Kumar, Phys. Rev. D **84**, 077301 (2011).
19. S. Dev, S. Gupta, and R. R. Gautam, Phys. Lett. B **701**, 605 (2011).
20. T. Araki, J. Heeck, and J. Kubo, J. High Energy Phys. **07**, 083 (2012).
21. P. Ludle, S. Morisi, and E. Peinado, Nucl. Phys. B **857**, 411 (2012).
22. E. Lashin and N. Chamoun, Phys. Rev. D **85**, 113011 (2012).
23. K. Deepthi, S. Gollu, and R. Mohanta, Eur. Phys. J. C **72**, 1888 (2012).
24. D. Meloni and G. Blankenburg, Nucl. Phys. B **867**, 749 (2013).
25. D. Meloni, A. Meroni, and E. Peinado, Phys. Rev. D **89**, 053009 (2014).
26. S. Dev, R. R. Gautam, L. Singh, and M. Gupta, Phys. Rev. D **90**, 013021 (2014).
27. R. G. Felipe and H. Serodio, Nucl. Phys. B **886**, 75 (2014).
28. P. O. Ludl and W. Grimus, J. High Energy Phys. **07**, 090 (2014).
29. L. M. Cebola, D. E. Costa, and R. G. Felipe, Phys. Rev. D **92**, 025005 (2015).
30. R. R. Gautam, M. Singh, and M. Gupta, Phys. Rev. D **92**, 013006 (2015).
31. S. Dev, L. Singh, and D. Raj, Eur. Phys. J. C **75**, 394 (2015).

32. T. Kitabayashi and M. Yasuè, Phys. Rev. D **93**, 053012 (2016).
33. S. Zhou, Chin. Phys. C **40**, 033102 (2016).
34. M. Singh, G. Ahuja and M. Gupta, Prog. Theor. Exp. Phys. **2016**, 123B08 (2016).
35. T. Kitabayashi, and M. Yasuè, Int. J. Mod. Phys. A **32**, 1750034 (2017).
36. T. Kitabayashi, S. Ohkawa and M. Yasuè, Int. J. Mod. Phys. A **32**, 1750186 (2017).
37. K. Bora, D. Borah and D. Dutta, Phys. Rev. D **96**, 075006 (2017).
38. D. M. Barreiros, R. G. Felipe and F. R. Joaquim, Phys. Rev. D **97**, 115016 (2018).
39. T. Kitabayashi, Phys. Rev. D **98**, 083001 (2018).
40. D. M. Barreiros, R. G. Felipe and F. R. Joaquim, J. High Energy Phys. **01**, 223 (2019).
41. T. Kitabayashi, Int. J. Mod. Phys. A **34**, 1950098 (2019).
42. F. Capozzi, E. D. Valentino and E. Lisi, A. Marrone, A. Melchiorri and A. Palazzo, Phys. Rev. D **101**, 116013 (2020).
43. M. Singh, EPL **2020**, 11002 (2020).
44. D. M. Barreiros, F. R. Joaquim and T. T. Yanagida, Phys. Rev. D **102**, 055021 (2020).
45. T. Kitabayashi, Phys. Rev. D **102**, 075027 (2020).
46. T. Fukuyama and H. Nishiura, (1997), arXiv:hep-ph/9702253.
47. C. S. Lam, Phys. Lett. B **507**, 214 (2001).
48. E. Ma and M. Raidal, Phys. Rev. Lett. **87**, 011802 (2001); Erratum Phys. Rev. Lett. **87**, 159901 (2001).
49. K. R. S. Balaji, W. Grimus, and T. Schwetz, Phys. Lett. B **508**, 301 (2001).
50. Y. Koide, H. Nishiura, K. Matsuda, T. Kikuchi, and T. Fukuyama, Phys. Rev. D **66**, 093006 (2002).
51. T. Kitabayashi and M. Yasue, Phys. Rev. D **67**, 015006 (2003).
52. Y. Koide, Phys. Rev. D **69**, 093001 (2004).
53. I. Aizawa, M. Ishiguro, T. Kitabayashi, and M. Yasue, Phys. Rev. D **70**, 015011 (2004).
54. A. Ghosal, Mod. Phys. Lett. A **19**, 2579 (2004).
55. R. N. Mohapatra and W. Rodejohann, Phys. Rev. D **72**, 053001 (2005).
56. Y. Koide, Phys. Lett. B **607**, 123 (2005).
57. T. Kitabayashi and M. Yasue, Phys. Lett. B **621**, 133 (2005).
58. N. Haba and W. Rodejohann, Phys. Rev. D **74**, 017701 (2006).
59. Z. Z. Xing, H. Zhang, and S. Zhou, Phys. Lett. B **641**, 189 (2006).
60. Y. H. Ahn, S. K. Kang, C. S. Kim, and J. Lee, Phys. Rev. D **73**, 093005 (2006).
61. A. S. Joshipura, Eur. Phys. J. C **53**, 77 (2008).
62. J. C. Gomez-Izquierdo and A. Perez-Lorenzana, Phys. Rev. D **82**, 033008 (2010).
63. H. J. He and F. R. Yin, Phys. Rev. D **84**, 033009 (2011).
64. H. J. He and X. J. Xu, Phys. Rev. D **86**, 111301 (2012).
65. J. C. Gomez-Izquierdo, Eur. Phys. J. C **77**, 551 (2017).
66. T. Fukuyama, Prog. Theor. Exp. Phys. **2017**, 033B11 (2017).
67. T. Kitabayashi, Int. J. Mod. Phys. A **31**, 09 (2016).
68. T. Kitabayashi and M. Yasuè, Phys. Rev. D **94**, 075020 (2016).
69. Z. H. Zhao, X. Y. Zhao, and H. C. Bao, Phys. Rev. D **105**, 035011 (2022).
70. E. A. Garcés, Juan Carlos Gómez-Izquierdo and F. Gonzalez-Canales Eur. Phys. J. C **78**, 812 (2018).
71. Juan Carlos Gómez-Izquierdo and Myriam Mondragón Eur. Phys. J. C **79**, 285 (2019).
72. Juan Carlos Gómez-Izquierdo and Adble Pérez-Lorenzana, Phys. Rev. D **77**, 113015 (2008).
73. Shao-Feng Ge, Hong-Jian He, and Fu-Rong Yin, J. Cosmol. Astropart. Phys. **05**, 017 (2010).
74. Hong-Jian He, Werner Rodejohann and Xun-Jie Xu, Phys. Lett. B **751**, 586-594 (2015).

42 *Y. Chen, Y. Hyodo, and T. Kitabayashi*

75. Juan Carlos Gómez-Izquierdo, F. Gonzalez-Cannles and M. Mondragón, Int. J. Mod. Phys. A **32**, 1750171 (2017).
76. Stefan Antusch, Stephen F. King, Christoph Luhn, and Martin Sprinrath, Phys. Lett. B **856**, 328-341 (2012).
77. J. D. Garcia-Aguilan, A. E. Poza Ramirez, M. M. Suárez Castañeda, and J. C. Gómez-Izquierdo, Revista Mexicana de Fisica. **69**, 030802 (2023).
78. Y. Hyodo and T. Kitabayashi, Prog. Theor. Exp. Phys. **2021**, 123B08 (2021).
79. P. F. Harrison and W. G. Scott, Phys. Lett. B **594**, 324 (2004).
80. C. S. Lam, Phys. Lett. B **640**, 260 (2006).
81. R. R. Gautam and S. Kumar, Phys. Rev. D **94**, 036004 (2016).
82. M. J. S. Yang, Prog. Theor. Exp. Phys. **2022**, 013B12 (2022).
83. K. S. Channey and S. Kumar, J. Phys. G: Nucl. Part. Phys. **46**, 015001 (2019).
84. S. Verma and M. Kashav, J. Phys. G: Nucl. Part. Phys. **47**, 085003 (2020).
85. M. Kashav, L. Singh and S. Verma arXiv:2207.13328.
86. Y. Hyodo and T. Kitabayashi, Int. J. Mod. Phys. A **35**, 2050183 (2020).
87. G. Altarelli and F. Feruglio, Rev. Mod. Phys. **82**, 2701 (2010).
88. C. S. Lam, Phys. Rev. D **74**, 113004 (2006).
89. X. G. He and A. Zee, Phys. Lett. B **645**, 427 (2007).
90. X. G. He and A. Zee, Phys. Rev. D **84**, 053004 (2011).
91. C. H. Albright and W. Rodejohann, Eur. Phys. J. C **62**, 599 (2009).
92. C. H. Albright, A. Dueck, and W. Rodejohann, Eur. Phys. J. C **70**, 1099 (2010).
93. J. D. Bjorken, P. F. Harrison, and W. G. Scott, Phys. Rev. D **74**, 073012 (2006).
94. S. Kumar, Phys. Rev. D **82**, 013010 (2010).
95. S. Kumar, Phys. Rev. D **88**, 016009 (2013).
96. M. J. S. Yang, Nucl. Phys. B **982**, 115893 (2022).
97. W. Grimus, and L. Lavoura, J. High Energy Phys. **09**, 106 (2008).
98. W. Grimus, L. Lavoura, and A. Singraber, Phys. Lett. B **686**, 141 (2010).
99. S. Morisi, Ketan M. Patel, and E. Peinado, Phys. Rev. D **84**, 053002 (2011).
100. C. Luhn, Nucl. Phys. B **875**, 80 (2013).
101. W. Rodejohann, and X.-J. Xu, Phys. Rev. D **96**, 055039 (2017).
102. R. R. Gautam, Phys. Rev. D **97**, 055022 (2018).
103. Z.-h. Zhao, X.-Y. Zhao, and H.-C. Bao, Phys. Rev. D **105**, 035011 (2022).
104. M. Blennow, P. Coloma, E. F.-Martinez, J. H.-Garciac, and J. L.-Pavone, J. High Energy Phys. **04**, 153 (2017).
105. F. J. Escrivuela, D. V. Forero, O. G. Miranda, M. Tórtola, and J. W. F. Valle, Phys. Rev. D **92**, 053009 (2015).
106. F. J. Escrivuela, D. V. Forero, O. G. Miranda, M. Tórtola, and J. W. F. Valle, New. J. Phys. **19**, 093005 (2017).
107. D. V. Forero, C. Giunti, C. A. Ternes, and M. Tórtola, Phys. Rev. D **104**, 075030 (2021).
108. S. Gariazzo, M. Gerbino, T. Brinckmann, M. Lattanzi, O. Mena, T. Schwetz, S. R. Choudhury, K. Freese, S. Hannestad, C. A. Ternes, and M. Tórtola, J. Cosmol. Astropart. Phys. **03**, 046 (2023).
109. B. Pontecorvo, Sov. Phys. JETP 6 (1957) 429.
110. B. Pontecorvo, Sov. Phys. JETP 7 (1958) 172.
111. Z. Maki, M. Nakagawa and S. Sakata, Prog. Theor. Phys. **28**, 870 (1962).
112. R. L. Workman *et al.* (Particle Data Group), Prog. Theor. Exp. Phys. **2022**, 083C01 (2022).
113. C. Jarlskog, Phys. Rev. Lett. **55**, 1039 (1985).
114. I. Esteban, M. C. Gonzalez-Garcia, M. Maltoni, T. Schwetz, and A. Zhou J. High

Modified trimaximal mixing for solar and reactor neutrino mixing angles 43

Energy Phys. **09**, 178 (2020). See also, NuFIT 5.2 (2022), www.nu-fit.org.